9

Midlatitude Cloud Systems

GEORGE TSELIOUDIS & KEVIN GRISE

In contrast to the tropics and subtropics, the middle latitudes are characterised by large meridional temperature gradients, created as a consequence of differential radiative heating between high and low latitudes. These meridional temperature gradients often concentrate in relatively narrow baroclinic zones that become unstable to wave-like perturbations called baroclinic eddies, or more commonly baroclinic storms or midlatitude cyclones. Baroclinic storms constitute the primary source of poleward energy transport at midlatitudes, which is accomplished through contrasting transports of warm air masses poleward (warm fronts) and cold air masses equatorward (cold fronts). Baroclinic storms also flux momentum into midlatitude regions, driving a region of enhanced westerly winds from the surface to the upper troposphere called the eddy-driven jet stream.

Baroclinic storms are the primary source of midlatitude cloud formation, and thus play an important role in determining the radiative and hydrologic budgets in midlatitude regions. High clouds of various vertical extents tend to form in the uplift regimes of the warm and cold fronts associated with the baroclinic storms, while low cloud decks often form in the subsidence regimes of the cold air masses that follow a cold frontal passage. As a result, the midlatitude cloud field encompasses almost the full range of cloud types, and the appearance of particular cloud types can be viewed as a tracer of midlatitude dynamic regimes. Because the clouds in the vicinity of the warm and cold fronts tend to be optically thick and often have tops in upper tropospheric layers, they produce substantial shortwave and longwave radiative signatures. Section 1.2.1 and Chapter 4 provide a detailed review of the shortwave and longwave radiative signatures of clouds. Briefly, the large optical depth of the clouds in the vicinity of the fronts promotes the reflection of incident solar radiation (a shortwave cooling effect), whereas the cold cloud top temperatures promote the reduction of outgoing longwave radiation to space (a longwave warming effect). In contrast, the low cloud decks in midlatitude cold air regimes have primarily a shortwave cooling effect, as their cloud-top temperature differs little from the underlying surface temperature.

These shortwave cooling and longwave warming effects make midlatitude clouds a key contributor to the global radiative budget and thus a potential source of significant radiative feedbacks in climate change situations (Chapter 13). Changes in the climate system, such as a climate warming, could affect meridional temperature gradients as well as the moisture availability of the atmosphere, which, through latent heat release, constitutes an additional energy source for baroclinic storms. Consequently, significant changes in the track and strength of baroclinic storms could occur with climate warming, and these changes would alter the midlatitude cloud field and produce radiative and hydrologic climate feedbacks. At the same time, altered cloud fields through their radiative effects and latent heat release have the ability to change temperature gradient patterns which in return can alter the characteristics of the midlatitude atmospheric circulation. The examination of midlatitude cloud processes and feedbacks, therefore, requires a detailed understanding of the relationships between the dynamical features of baroclinic storms and the properties of the clouds that they produce.

This Chapter will examine in detail the relationships between cloud properties and atmospheric dynamics in midlatitude regions. Cloud structures and formation mechanisms in baroclinic storms will be examined first, with an emphasis on the latest satellite retrievals of cloud properties. Next, the climatologies of midlatitude clouds and their radiative properties will be discussed. Then the interactions of the midlatitude atmospheric circulation with clouds and their radiative properties will be examined, including an examination of the effects of clouds on the midlatitude circulation. Finally, the Chapter will address how midlatitude clouds may be affected in a changing climate.

9.1 Midlatitude cloud structures

9.1.1 Cloud structures in baroclinic storms

Baroclinic storm clouds have been extensively observed from both ground sites and space-based platforms, as they are integrally linked to weather forecasting at midlatitudes. Since the early days of weather observations, attempts have been made to explain the circulation features in a baroclinic storm and to map the cloud and precipitation structures that are formed in the different components of those circulation features. In this section, a brief description will be provided of early theories that explain the dynamical circulations and the resulting cloud formations in midlatitude storms, and then more recent results will be presented that use satellite retrievals, meteorological observations, and field campaign results to quantitatively characterise the properties of the

midlatitude cloud field and their relationship with midlatitude atmospheric dynamics.

9.1.1.1 Norwegian cyclone model

As early as the late 19th century, it was recognised that midlatitude baroclinic storms had a typical pattern in their cloudiness, such that systematic cloud observations might provide clues as to the development of weather systems. The first International Cloud Atlas published in 1896 allowed for the standardisation of remote cloud observations (Chapter 1). As a result of these early observations, the first conceptual model to depict the circulation and cloud features in a midlatitude cyclone, the Norwegian Cyclone Model, was formulated in the late 1910s and early 1920s by Jacob BjerknesindexBjerknes, Jacob [1]. The model was constructed through the accumulation of surface observations of a multitude of storm passages, which typically include the appearance first of the warm frontal sector with southerly winds and warm temperatures followed by the passage of the cold front that turns the winds to northerly directions and drops the temperatures significantly. A schematic of the model is shown in Fig. 9.1, where the warm and cold air circulation regimes that form the warm and cold frontal regions around a Northern Hemisphere low pressure centre are shown with arrows, and the typical cloud and precipitation types that occur in each regime are drawn schematically and noted using cloud classification definitions. The classification of cloud types is based on the definitions used by surface weather observers that have changed very little over time (see Chapter 1). Those types identified by the weather observers as the primary clouds in midlatitude storms, included thin cirrus (Ci) and cirrostratus (CiStr) clouds occurring upstream of the storm centre, nimbus clouds (Ni) together with rain or snow along the warm and cold frontal zones, and altostratus clouds (AStr) in the cold air mass behind the cold front.

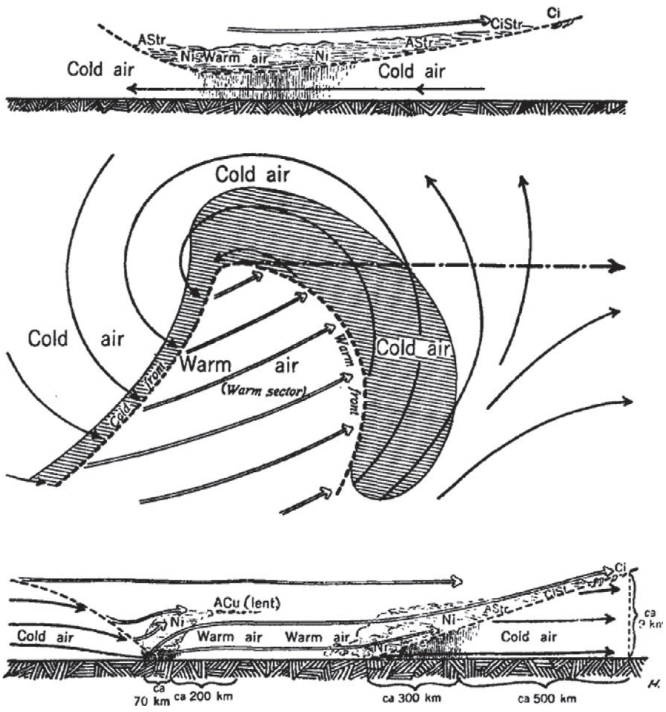

Figure 9.1 A schematic illustration of frontal clouds and precipitation constructed based on the Norwegian Cyclone Model, as conceptualised in the work of Bjerknes and Solberg (1922). The middle panel shows the warm and cold fronts and the movement of air around the storm centre, and the top and bottom plots show schematics of two west-east cross sections through the storm with indications of the locations of different cloud types, precipitation, and air movements. Adapted from Posselt et al. (2008). Copyright © 2008 American Meteorological Society. Used with permission.

9.1.1.2 Quasi-geostrophic theory

In the 1940s and 1950s, quasi-geostrophic theory was introduced, which helped to resolve with a high degree of accuracy the synoptic atmospheric motions associated with midlatitude baroclinic storms. A detailed explanation of quasi-geostrophic theory is provided in many atmospheric dynamics textbooks (see Further Reading at the end of the ../CHAPTER). A brief summary is provided here.

The quasi-static (primitive) equations describe the dynamics of large-scale flows in the atmosphere. The origin of these equations is discussed in detail in Section 2.4.2 of Chapter 2. Using pressure as a vertical coordinate, the horizontal momentum equations can be written concisely as:

$$\mathrm{D}_t \boldsymbol{v}_p = -\boldsymbol{f} \times \boldsymbol{v} - \nabla_p \phi, \tag{9.1}$$

where ϕ is the geopotential and $\mathrm{D}_t = \partial_t + \boldsymbol{v}_p \cdot \nabla_p$. In midlatitude synoptic-scale weather systems, a scale analysis of the terms in Eq. (9.1) reveals an approximate balance between the Coriolis force and pressure gradient force terms, which is referred to as geostrophic balance:

$$0 \approx -\boldsymbol{f} \times \boldsymbol{v} - \nabla_p \phi. \tag{9.2}$$

Likewise, the horizontal wind that reflects an exact balance between the Coriolis and pressure gradient forces is referred to as the geostrophic wind $\boldsymbol{v_g}$:

$$\boldsymbol{v_g} = \{u_g, v_g, 0\} = (1/\boldsymbol{f}) \times \nabla_p \phi. \tag{9.3}$$

To first order, the winds in midlatitude weather systems are dominated by their geostrophic component. The ageostrophic component of the wind, $\boldsymbol{v_a} = \boldsymbol{v} - \boldsymbol{v_g}$, is comparatively much smaller, usually by an order of magnitude. Using this knowledge, the primitive equations can be greatly simplified by assuming that midlatitude synoptic-scale flows are approximately (but not exactly) in geostrophic balance ($\boldsymbol{v} \approx \boldsymbol{v_g} >> \boldsymbol{v_a}$). This *quasi-geostrophic approximation* sim-

[1] **Jacob Aall Bonnevie Bjerknes** (1897–1975) was a Norwegian meteorologist, who is widely considered to be one of the pioneers of modern meteorology. His contributions range from his early work on the Norwegian cyclone model at the Geophysical Institute in Bergen, Norway to his later work on the general circulation and the El Niño-Southern Oscillation as a professor at the University of California at Los Angeles.

plifies the horizontal momentum equations (9.1) as follows:

$$\frac{\mathrm{d_g}\boldsymbol{v_g}}{\mathrm{d}t} = -f_0\mathbf{k}\times\boldsymbol{v_a} - (\beta y)\mathbf{k}\times\boldsymbol{v_g}. \tag{9.4}$$

Here, note that, in the quasi-geostrophic approximation, the total derivative D_t in Eq. (9.1) is replaced by $\frac{\mathrm{d_g}}{\mathrm{d}t} = \frac{\partial}{\partial t} + u_\mathrm{g}\frac{\partial}{\partial x} + v_\mathrm{g}\frac{\partial}{\partial y}$. In other words, advection is approximated by the horizontal advection by the geostrophic wind; any vertical advection is neglected. Note also that the Coriolis parameter $\boldsymbol{f} = \{0, 0, f\}$ has been replaced by $\{0, 0, f_0 + \beta y\}$ using the so-called Beta-plane approximation where $f_0 >> \beta y$.

Similarly, using pressure as a vertical coordinate, the thermodynamic equation (2.143) can be written concisely as:

$$\mathrm{D}_t T + \frac{\omega}{c_p}\partial_p\phi = \frac{Q}{c_p}. \tag{9.5}$$

Here, we assume a dry atmosphere, such that the rhs of Eq. (9.5) equals the diabatic heating rate Q divided by the specific heat of dry air at constant pressure ($c_p = 1004\,\mathrm{J\,kg^{-1}\,K^{-1}}$).

We can rewrite the thermodynamic equation (9.5) in terms of the dry potential temperature θ (2.46):

$$\frac{\partial T}{\partial t} + u\frac{\partial T}{\partial x} + v\frac{\partial T}{\partial y} - S_p\omega = \frac{Q}{c_p}, \tag{9.6}$$

where $S_p = -\frac{T}{\theta}\frac{\partial\theta}{\partial p}$ is a measure of the static stability of the atmosphere in pressure coordinates. Under the quasi-geostrophic approximation, Eq. (9.6) simplifies to:

$$\frac{\mathrm{d_g}T}{\mathrm{d}t} - S_{p_0}\omega = \frac{Q}{c_p}, \tag{9.7}$$

where the subscript zero indicates a reference state temperature profile that varies only in the vertical direction ($S_{p_0} = -\frac{T_0}{\theta_0}\frac{\partial\theta_0}{\partial p}$).

It is often convenient to express the quasi-geostrophic horizontal momentum equations (Eq. 9.4) in terms of the quasi-geostrophic relative vorticity $\zeta_\mathrm{g} = \frac{\partial v_\mathrm{g}}{\partial x} - \frac{\partial u_\mathrm{g}}{\partial y}$:

$$\frac{\mathrm{d_g}\zeta_\mathrm{g}}{\mathrm{d}t} = -f_0\left(\frac{\partial u_\mathrm{a}}{\partial x} + \frac{\partial v_\mathrm{a}}{\partial y}\right) - \beta v_\mathrm{g}. \tag{9.8}$$

Now, the quasi-geostrophic thermodynamic equation (Eq. 9.7) and vorticity equation (Eq. 9.8) can be combined to yield one diagnostic equation for vertical motions in midlatitude weather systems, the quasi-geostrophic omega equation (9.9):

$$\begin{aligned}\left(\nabla_p^2 + \frac{pf_0^2}{R_\mathrm{d}S_{p_0}}\frac{\partial^2}{\partial p^2}\right)\omega = &-\frac{1}{S_{p_0}}\nabla_p^2(-\boldsymbol{v_g}\cdot\nabla_p T)\\ &-\frac{pf_0}{R_\mathrm{d}S_{p_0}}\frac{\partial}{\partial p}[-\boldsymbol{v_g}\cdot\nabla_p(\zeta_\mathrm{g}+f)] - \frac{1}{S_{p_0}}\nabla_p^2\frac{Q}{c_p}.\end{aligned} \tag{9.9}$$

Assuming that the atmosphere is statically stable ($S_{p_0} > 0$), the term on the lhs of Eq. (9.9) behaves like the Laplacian of the vertical velocity (omega, ω). Recalling that the Laplacian operator can be approximated as a negative sign (particularly near minima or maxima in a scalar field), the lhs of Eq. (9.9) can be qualitatively interpreted as -ω, or rising motion. The first term on the rhs of Eq. (9.9) is related to the Laplacian of temperature advection by the geostrophic wind on constant pressure surfaces. This term implies that warm air advection is associated with -ω (rising motion) and cold air advection is associated with +ω (sinking motion). The second term on the rhs of Eq. (9.9) is related to the differential absolute vorticity ($\zeta_\mathrm{g} + f$) advection by the geostrophic wind on constant pressure surfaces. This term implies that cyclonic vorticity advection increasing with height (decreasing with pressure, $\frac{\partial}{\partial p}$) is associated with -$\omega$ (rising motion) and anticyclonic vorticity advection increasing with height is associated with +ω (sinking motion). Finally, the third term on the rhs of Eq. (9.9) is related to the diabatic heating rate, including effects from radiation and the latent heat of condensation. This term implies that diabatic heating is associated with -ω (rising motion) and diabatic cooling is associated with +ω (sinking motion). The diabatic heating term is often neglected, if air motions are assumed to be adiabatic .

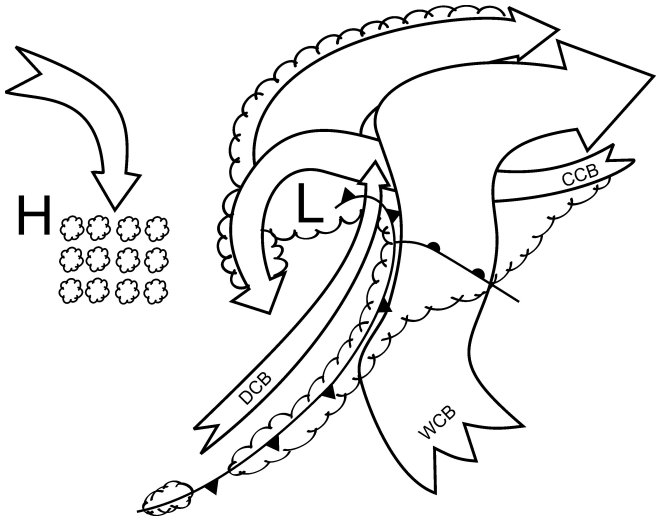

Figure 9.2 A schematic view of the conveyor belt model for the air circulation in midlatitude storm systems. The figure shows the positions of the fronts, the low-pressure centre (labeled as L), a high-pressure centre (labeled as H), and the three major conveyor belt circulations (warm conveyor belt: WCB, cold conveyor belt: CCB, and dry conveyor belt: DCB). The sense of circulation assumes $f > 0$ and would be reversed for $f < 0$, as in the Southern Hemisphere.

9.1.1.3 The "conveyor belt" model

Using knowledge from quasi-geostrophic theory, the Norwegian Cyclone Model can be extended into the so-called conveyor belt model, which is a full-scale model of the circulation, cloud, and precipitation components of baroclinic storms. The conveyor belt model is summarised in Fig. 9.2 and includes three major circulation features ("conveyor belts") surrounding the low-pressure centre of a baroclinic storm. Note that the latitudinal transports shown in Fig. 9.2 and discussed below apply to the Northern Hemisphere ($f > 0$) and must be reversed for Southern Hemisphere ($f < 0$) baroclinic storms.

The first feature of the conveyor belt model is a warm conveyor belt that originates at low levels in the southeastern quadrant of the storm and carries warm, moist air towards

the north. This warm, moist air mass is often convectively unstable and therefore produces convective clouds and precipitating systems, including squall lines and strong thunderstorms. Even in the absence of convection, however, the large scale lifting of the warm, moist air by the approaching cold front produces thick clouds with high tops that often precipitate. As the warm conveyor belt moves northward, this air motion is associated with warm air advection, and thus consistent with Eq. (9.9), the air rises as it flows northward and lifts over the warm front. This large-scale rising motion often produces large regions of stratiform cloud cover and precipitation ahead of the warm front. As the warm conveyor belt ascends, it is deflected to the east by the strong westerly winds in the midlatitude upper troposphere. As the warm conveyor belt moves to the east and northeast of the storm centre, the lifted moist air forms cirrostratus clouds that thin and change to cirrus as the air stream moves further eastward. Therefore, the appearance of cirrus clouds moving into a midlatitude region from the west is considered a harbinger of a storm passage.

The second circulation feature of the conveyor belt model is a cold conveyor belt that originates to the northeast of the low-pressure centre and brings cold air westward, as it passes underneath the warm conveyor belt and parallels the warm front along its northern edge. As the cold conveyor belt passes underneath the warm conveyor belt and warm frontal precipitation, it becomes significantly moistened and begins to rise slowly as it nears the low-pressure centre. The rising motion near the surface low is consistent with cyclonic vorticity advection increasing with height (from Eq. (9.9)), as an intensifying baroclinic weather system tilts westward with height such that the cyclonic vorticity advection associated with a mid-tropospheric trough (cyclonic vorticity anomaly) is typically positioned above the surface low. Once in the vicinity of the surface low, the cold conveyor belt splits into two branches: 1) an anticyclonic branch that is deflected eastward by the mid-tropospheric westerly winds and follows at lower levels the warm conveyor belt and 2) a cyclonic branch that wraps around the surface low, producing a distinctive comma-shaped cloud feature to the west of the surface low. Throughout its track, the low-level cold conveyor belt favours the formation of stratus cloud decks and fogs, which are often enhanced by evaporating precipitation falling from the warm conveyor belt above. Further to the west of the low-pressure centre, shallow cumulus cloud decks often form over ocean, as the cold air advection from the cyclonic circulation of air passes over warmer ocean waters.

The final circulation feature of the conveyor belt model is a dry conveyor belt. The dry conveyor belt originates in the upper troposphere and descends cyclonically to the south of the surface low, creating a dry tongue, or dry slot, at the western edge of the cold frontal circulation. The descending motion of the dry conveyor belt behind the cold front is consistent with the cold air advection occurring in this region (from Eq. (9.9)).

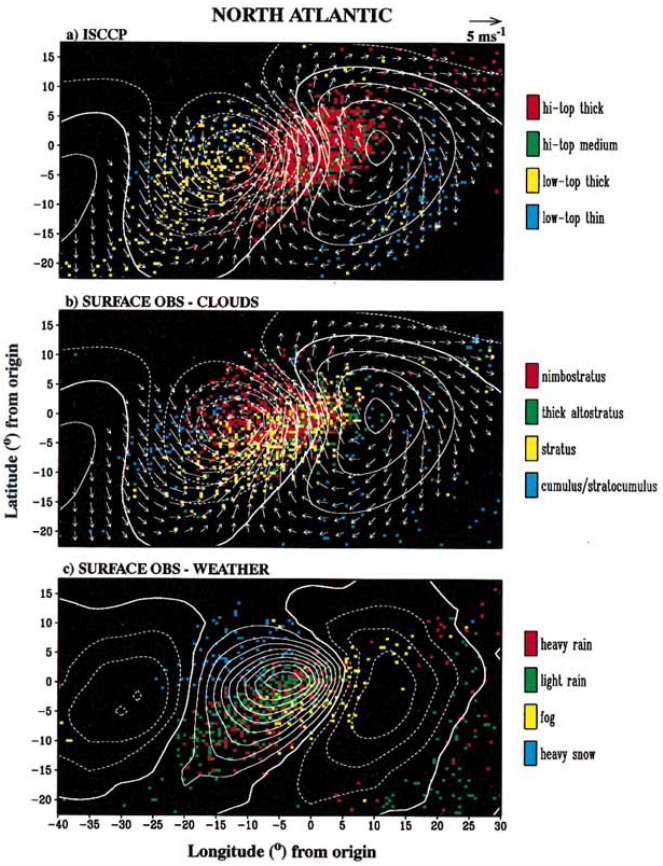

Figure 9.3 Patterns of the amount of selected cloud types based on (a) ISCCP data and (b) surface observations, and (c) frequency of occurrence of selected surface weather types, for a composite of midlatitude storms over the North Atlantic during the cool season (October–March). The colours on the plots indicate the relative abundance of a cloud type or weather regime as they are listed on the right of each plot, while the arrows (see scaling at top right) and contours (interval: 10 m) in (a) and (b) indicate the composite anomalous 1000 hPa wind and geopotential height fields from European Centre for Medium-Range Weather Forecasts (ECMWF) analyses, respectively. The composite anomaly pattern for the vertical velocity ω (with positive values indicating upward motion) from the ECMWF data is shown as contours (interval: 2×10^{-2} Pa s^{-1}) in (c). Solid (dashed) contours indicate positive (negative) values. Adapted from Lau and Crane (1997).

9.1.1.4 Satellite retrievals of storm cloud properties

Surface weather observers provided these first, qualitative descriptions of the cloud structures in midlatitude baroclinic storms. Since the early 1980s, retrievals of cloud, radiation, and precipitation properties from satellite instruments have started to provide more quantitative information about the radiative and hydrologic structures of the global cloud field. Satellite retrievals provide detailed properties of midlatitude clouds and therefore make it possible to quantitatively relate those properties to the properties of the baroclinic storms that constitute the primary mechanism for the formation of these clouds.

A composite of satellite and surface retrievals of cloud and precipitation properties in a baroclinic storm is shown in Fig. 9.3. The satellite cloud property retrievals come from the International Satellite Cloud Climatology Project (ISCCP) while the cloud type and weather type observations come from surface weather observers (see Chapter 1 for a detailed discussion of cloud observing systems). The figure shows a composite for cyclones over the North Atlantic, for the ISCCP cloud type retrievals (top), the surface observers' cloud types (middle), and the surface observers' weather types (bottom). The satellite definition of cloud height is based on a satellite measurement of the thermal emission from the top of the cloud, which indicates the temperature and therefore the vertical location of the cloud radiative top. The definition of cloud optical thickness is based on the cloud reflectance of solar radiation, which is indicative of the vertical thickness of the cloud and the density of the water and/or ice in it (Chapter 3). It is remarkable that the classical view of the cloud distribution around baroclinic storms derived first by surface observers as early as the late 19th century (Fig. 9.1) is verified with high accuracy by the global satellite retrievals and the more recent surface observer data; high-top thick and high-top medium or nimbostratus and altostratus clouds along with heavy precipitation dominate the warm and cold frontal regions of the storm, while low-top thick and low-top thin or stratus and cumulus/stratocumulus clouds along with snow are found in the cold air outbreak region behind the storm. One major difference between the surface observers and the satellite cloud types relates to the fact that the surface observers find large amounts of stratus cloud in the frontal sectors where the satellite retrieves higher top thick clouds. This is due to the bottom-up view of the surface observers versus the top-down view of the satellite and the fact that cloud top is not readily retrievable from the surface when the sky is fully covered by cloud.

The cloud structures derived by surface observers and by the first satellite cloud retrievals provide an illustration of the average structure of cloud type distribution in a typical midlatitude storm. However, cloud cover and cloud type distributions tend to vary widely both with changes in the strength of the baroclinic storms as well as with changes in atmospheric conditions that the storm is embedded in, such as the moisture availability of the atmosphere. In recent years, the global, multi-year nature of satellite observations along with reconstructions of atmospheric conditions by reanalysis datasets, allow us to analyse large ensembles of baroclinic storms and to derive meaningful classifications that make it possible to examine how the cloud structures and properties change with changing dynamic and thermodynamic conditions. Fig. 9.4 illustrates the change in high clouds in midlatitude storms with changing storm strength (horizontal axis) and moisture availability of the atmospheric column (vertical axis). Here the strength of the storm is measured by the pressure value of the storm's low pressure centre. It can be seen that the amount of high cloud in a storm is strongly dependent on the storm strength since, for the same atmospheric moisture conditions, high clouds become more abundant and cover a larger region along the cold and warm frontal zones as the storm strength increases. The

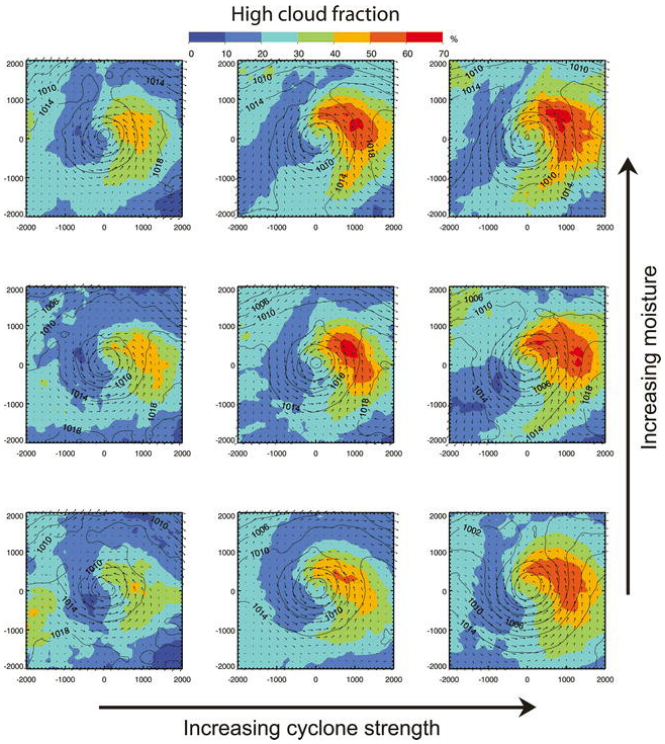

Figure 9.4 Composites of the amount of high cloud from midlatitude storms (cyclones) in all the major storm tracks, classified by the cyclone strength (increasing left to right) and the atmospheric moisture (increasing bottom to top). Cyclone strength is defined as the mean wind speed within 2000 km of the low-pressure centre and the atmospheric moisture as the mean precipitable water within 2000 km of the low-pressure centre. The composite mean surface pressure contours (in hPa) and surface wind vectors are also shown. Adapted from Field and Wood (2007). Copyright © 2007 American Meteorological Society. Used with permission.

dependence of high cloud amount on atmospheric moisture availability is much weaker than the dependence on storm strength.

The first generation of satellite observations included cloud imagers that were able to retrieve cloud properties such as cloud top temperature and optical depth from radiances and irradiances originating from the cloud top. These measurements provided information on the column-mean cloud properties but did not provide information on the vertical variability of the cloud layers. The advent of active remote sensing measurements from space with the launch of the CloudSat radar and the lidar, CALIOP, in 2006 made it possible to examine the vertical distribution of cloud layers in the vicinity of baroclinic storms. Fig. 9.5 shows a cross-section of the vertical profile of cloud layers in a baroclinic storm over the North Atlantic, derived from CloudSat radar retrievals. It can be seen that there is again a remarkable similarity of vertical structure with the cross-section of the cloud vertical profiles derived by the Norwegian cyclone model some 80 years earlier and shown in Fig. 9.1. The cloud type progression during the storm passage, with the cirrus and cirrostratus clouds ahead of the storm, the nimbostratus clouds along the frontal zones, and the low-top post-frontal clouds, is now

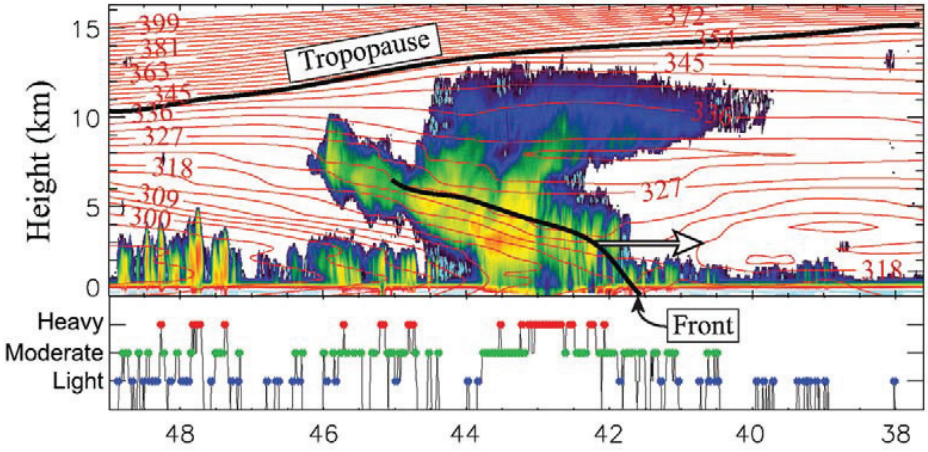

Figure 9.5 Cross-section along a North Atlantic baroclinic storm of CloudSat observed radar reflectivity (dBZ, colour shaded), overlaid with ECMWF-analysed equivalent potential temperature (K, solid red lines). The positions of the cold front and tropopause are marked with heavy black lines, and the direction of movement of the front is indicated with a white arrow. CloudSat-estimated precipitation rate is depicted directly below the plot of observed reflectivity. Adapted from Posselt et al. (2008). Copyright © 2008 American Meteorological Society. Used with permission.

verified through the use of radar retrievals. However, the use of active remote sensing also makes clear the existence of multi-layered clouds in the storm, a detail that cannot be readily resolved either from passive remote sensing or from surface observations. The pre-frontal cirrus are accompanied by low thin cloud decks, while part of the cold frontal clouds are formed by two distinct thick layers of low and high cloud tops. This explains the difference in the view of the frontal clouds between satellite and surface observations shown in Fig. 9.3.

9.1.2 Regional patterns of midlatitude cloud organisation

The observational analyses presented so far show that, at synoptic scales, baroclinic storm systems constitute a major source of the variety of cloud types, and that cloud cover and type varies significantly depending on location within the baroclinic storm domain. High clouds dominate the warm conveyor belt circulation while low clouds occur in the cold conveyor belt. When averaged to form a climatology, however, the midlatitude cloud field does not show the pronounced regional patterns found in other climate regimes, other than some distinct cloud cover differences between land and ocean in the Northern Hemisphere. This relative uniformity of the midlatitude cloud field is due to the transient nature of baroclinic storms, which tend to distribute cloud amounts in a somewhat uniform manner throughout the three major oceanic storm tracks, located across the North Atlantic, North Pacific, and Southern Oceans.

The midlatitude storm tracks have been thoroughly documented and studied for well over a century, as they constitute the major weather makers for many of the world's populated regions. Midlatitude storms are commonly tracked by following the movement of the low-pressure centre that constitutes the centre of the storm over the duration of a storm's lifecycle (from cyclogenesis to cyclolysis). Storm tracking can either be performed manually (by hand) or through the use of an automated computer algorithm, which applies propagation and direction criteria to follow a low-pressure centre. Fig. 9.6 shows two maps of the North Atlantic storm track, the top map coming from the climatology atlas published by Wladimir Köppen[2] in 1882 and the bottom map coming from the application of a storm tracking algorithm on sea level pressure data over the years 2000–2015. It is remarkable to note the similarities between the two maps, given the sparse observational network available near the end of the 19th century. Several centres of large storm activity are present in both maps, including the maximum between Greenland and Iceland (the Icelandic Low) and the secondary storm track in the Mediterranean region. The location of the storm track is not necessarily stationary in time. There is some evidence that suggests that the North Atlantic storm track shifted poleward over the latter half of the 20th century. The potential effects of this storm track shift on the cloud field and its radiative effects are discussed in Section 9.3.1.

Some of the highest cloud amounts on the planet are observed in the midlatitude storm tracks (see Fig. 4.6 in Section 4.5.1). In the three major oceanic storm tracks, annual mean total cloud cover is almost everywhere higher than 70%, and shows only weak regional patterns over the Northern Hemisphere oceans. In those basins, cloud cover tends to be higher in the western parts, maintaining values above 80% especially in the winter season when the storm tracks are generally most active. These larger cloud covers are caused by larger amounts of high-top clouds in the western basins, while low cloud amounts are somewhat higher in the eastern

[2] **Wladimir Köppen** (1846–1940) was a Russian-born climatologist, who spent much of his professional career at the German Naval Observatory in Hamburg. He is best known for establishing the Köppen classification of the world's climate zones, but was also an author on the first International Cloud Atlas (see Section 1.1.1).

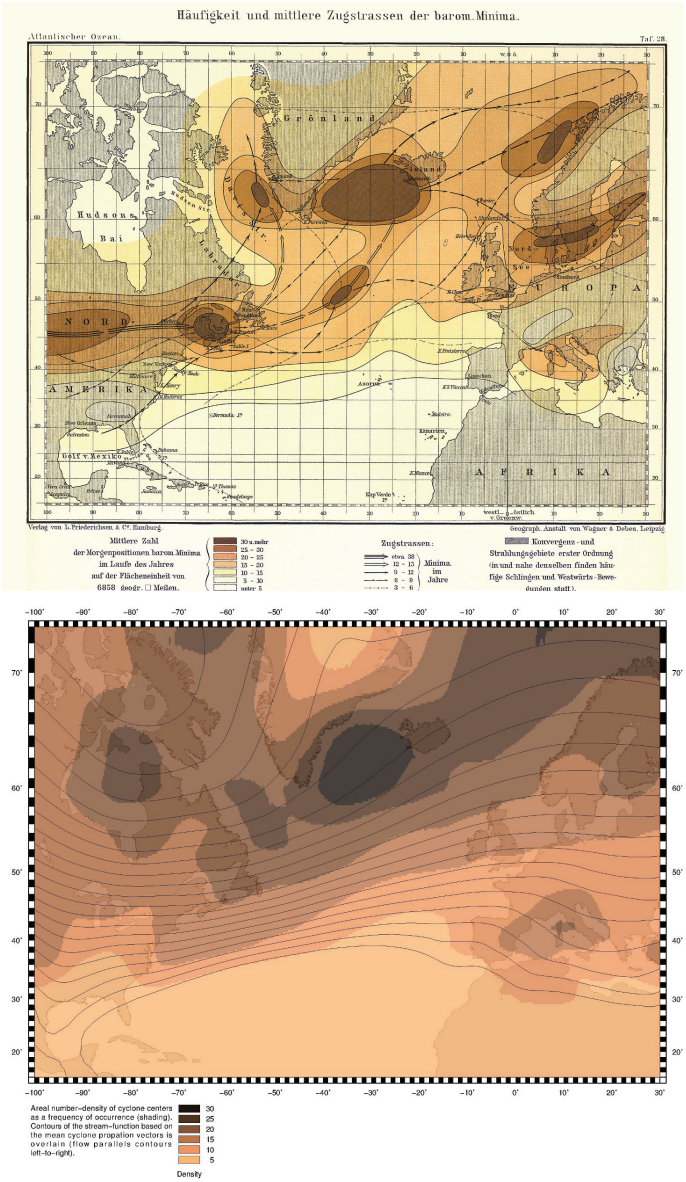

Figure 9.6 (Top) Frequency of surface lower pressure centres (colours) and density of centre paths (arrows) over the course of a year from the 1882 Köppen climatology atlas. (Bottom) Areal number density of cyclone centres (colours) and stream function of mean cyclone propagation from a 15-year climatology (2000–2015), derived using the storm tracking analysis of Bauer et al. (2016).

parts of the Northern Hemisphere ocean basins. The western parts of the basins are the cyclogenesis areas of the oceanic storm tracks (Hoskins and Hodges, 2002), and storms tend to produce larger amounts of high clouds in their formation stages than in their decay stages. Low cloud decks, on the other hand, occur more frequently in the eastern parts of the basins, because a) the subtropical and lower midlatitude parts of the Eastern North Atlantic are dominated by the semi-permanent Azores high pressure system, which tends to deflect storm tracks to the north (Fig. 9.6) and favours the formation of stable boundary layers and stratocumulus cloud decks, and b) in the eastern North Pacific, cold surface waters favour the formation of fogs and stratocumulus clouds through mechanisms explained in more detail in Chapter 8.

Midlatitude continental total cloud cover ranges in the annual mean between 40% and 70% and is, therefore, significantly lower than the midlatitude oceanic cloud cover. This is true for all cloud types with the exception of high thin cirrus clouds. The overall lower continental cloud covers are due both to the smaller moisture supply of the land compared to the ocean surface and to the overall weaker storm systems occurring over land. The continental storm tracks also tend to have smaller frequencies of storm systems than the oceanic storm tracks, partly because of shorter-lived storms over land. These factors contribute to the lower cloud cover over midlatitude continents.

The large amounts of midlatitude continental cirrus clouds are primarily orographic in nature. Orographic cloud formation occurs preferably on the leeward side of mountain ranges, as eastward flowing air is lifted by the mountains and cools forming cloud layers throughout the extent of the resulting gravity wave. Orographic cirrus coverage can reach values of about 30%, thus constituting a major contributor to the total cloud cover in regions downwind from major mountain ranges, such as the Rocky Mountains in North America, the Andes Mountains in South America, and the Himalayas in Asia.

9.2 Effects of midlatitude clouds on the atmospheric radiation budget

In the climatology, midlatitude clouds exert stronger effects on the Earth's top-of-atmosphere (TOA) radiative budget than clouds in any other latitude band. Annual mean shortwave cloud radiative cooling at TOA in the midlatitude regions ranges between 30–90 $\mathrm{W\,m^{-2}}$, and these values are some of the largest observed on the planet, comparable only to the values found in the tropical Western Pacific warm pool region, Intertropical Convergence Zone (ITCZ), and the stratocumulus regions of the eastern subtropical ocean basins (Fig. 4.8). Midlatitude longwave cloud radiative warming ranges between 20–50 $\mathrm{W\,m^{-2}}$, lower only than the values observed in the ITCZ, the tropical Western Pacific, and the deep convective regions in the Amazon and equatorial Africa (Fig. 4.8). As a result, net cloud radiative cooling in the midlatitudes ranges between 10–40 $\mathrm{W\,m^{-2}}$, only rivalled by the net cloud radiative cooling in the stratocumulus regimes in the eastern subtropical ocean basins (Figs. 4.8 and 4.9). The large radiative cooling effect of midlatitude clouds makes them a significant contributor to the equator-to-pole temperature difference and hence acts to strengthen the large-scale atmospheric circulation (see Section 9.3.2).

As mentioned in the previous section, the transient nature of baroclinic storms distributes clouds, and therefore their radiative effects, rather uniformly along the major storm tracks. Large regional differences occur mainly between Northern Hemisphere land and ocean regions. Shortwave cloud radiative cooling over land ranges between 30–

$60\,\mathrm{W\,m^{-2}}$ while over ocean it ranges between 40–$90\,\mathrm{W\,m^{-2}}$. Shortwave cooling maxima occur in the cyclogenesis regions in the western parts of Northern Hemisphere ocean basins, and relative minima in shortwave cooling occur in the cyclolysis regions in the eastern parts of the ocean basins (Fig. 4.8). Cloud longwave warming over land ranges between 20–$40\,\mathrm{W\,m^{-2}}$ with the maxima occurring in the cirrus prone regions downwind from the Andes, the Rockies, and the Himalayas. Cloud longwave warming over ocean ranges between 30–$50\,\mathrm{W\,m^{-2}}$ with the maxima occurring in the high-cloud prone cyclogenesis regions (Fig. 4.8). The values listed here are annual mean values. However, in the midlatitudes, cloud radiative effects vary significantly with season, both because of seasonal storm track variability and the significantly lower solar insolation during the winter season. The lower insolation during winter reduces the wintertime shortwave cloud radiative effect, as by definition, a cloud of a certain optical depth will reflect less solar radiation in the winter than in the summer.

It is important to note here that the two components of the cloud radiative effect, the shortwave cooling and the longwave warming, manifest themselves at different heights in the atmospheric column. Shortwave cooling manifests itself at the surface and, therefore, affects surface-atmosphere energy exchanges and temperature gradients in the boundary layer. The longwave warming, on the other hand, manifests itself in the atmospheric column with emphasis on the upper troposphere. As a result, longwave warming, along with latent heat release, plays a significant role in the vertical distribution of energy exchanges and in determining temperature gradients in the upper troposphere. The customary addition of the shortwave and longwave cloud radiative effects to yield a net TOA cloud radiative effect does not properly resolve the different nature of the two contrasting effects, and is only useful in determining the net cloud contribution to the overall atmospheric energy budget. A net zero TOA cloud radiative effect that arises from the cancellation of contrasting shortwave and longwave cloud radiative effects implies vertical heating gradients that will be balanced by atmospheric circulation changes, which in turn can alter the cloud field and affect the radiative budget. Therefore, a net zero TOA cloud radiative effect does not necessarily correspond to a state of radiative equilibrium.

At the synoptic scale, large cloud radiative effect differences occur among the different circulation regimes of baroclinic storms. The existence of clouds with different cloud top heights and optical depths in the different storm sectors creates distinct radiative signatures. One way to understand these signatures is to separate the cloud radiative effects into instances when the sea level pressure (SLP) is higher and lower than the climatological value. This separation captures the climatological signatures of high and low pressure regimes, respectively. Combined analysis of recent satellite observations and weather data shows that the shortwave flux differences between high and low SLP regimes are significant and can vary with season: in the winter an excess shortwave cooling of 5–$20\,\mathrm{W\,m^{-2}}$ occurs in the low SLP regime while in the summer this excess cooling increases to 20–$50\,\mathrm{W\,m^{-2}}$, mostly due to the higher amounts of solar insolation (Tselioudis et al., 2000). This excess cooling manifests itself at the surface and would act to stabilise the surface horizontal temperature gradients in the storm, as it occurs primarily in the warm sector of the storm. The longwave differences between high and low SLP regimes are uniform across seasons and show an excess longwave warming of 5–$35\,\mathrm{W\,m^{-2}}$ in the low SLP regime. This excess warming is manifested mostly as an additional warming of the atmospheric column and would act to increase the upper tropospheric temperature gradients of the storm, as it occurs again in the warm sector of the storm.

9.3 Interaction of clouds with the midlatitude circulation

The results presented in the previous sections show that, at synoptic scales, the amount and type of cloud produced in a storm, and therefore the cloud radiative effect, depend on the strength of the storm and the moisture availability of the atmosphere (Fig. 9.4). This implies that changes in the strength of the midlatitude circulation or the atmospheric moisture content will initiate changes in the properties of the midlatitude cloud field that have the potential to produce strong cloud radiative feedbacks. Clouds, on the other hand, can also alter the atmospheric thermal structure through their diabatic effects, which can then impact the strength of the midlatitude baroclinic circulation. Hence, changes in the atmospheric circulation can modify clouds, and changes in clouds can in return modify the atmospheric circulation.

For a discussion of the interaction of midlatitude clouds with the atmospheric circulation, it is crucial, therefore, to examine in brief the properties and processes of the midlatitude atmosphere that determine the strength and character of its circulation. From the theoretical perspective, if one considers a purely zonal jet stream with geostrophic wind speed U_g that only depends on height z, then a suitable measure of the baroclinicity of the flow is the Eady growth-rate maximum:

$$\sigma_\mathrm{BI} = 0.31 \frac{f}{N} \left| \frac{\mathrm{d}U_\mathrm{g}}{\mathrm{d}z} \right|, \tag{9.10}$$

where f is the Coriolis parameter, and N is the Brunt-Väisälä frequency, a measure of the atmospheric static stability (Eq. (2.90); Table 2.7). The coefficient of 0.31 is derived from numerical calculations (Lindzen and Farrell, 1980).

Assuming hydrostatic balance (Eq. 2.136), the geostrophic wind (Eq. 9.3) varies with height according to the thermal wind relationship:

$$\frac{\partial \boldsymbol{v_\mathrm{g}}}{\partial z} = \frac{g}{\boldsymbol{f}} \times \nabla(\ln T). \tag{9.11}$$

Substituting for $\frac{\mathrm{d}U_\mathrm{g}}{\mathrm{d}z}$ from Eq. (9.11), the maximum Eady growth rate can be written in terms of the magnitude of the meridional temperature gradient $\frac{\partial T}{\partial y}$:

$$\sigma_\mathrm{BI} = 0.31 \frac{g}{TN} \left| \frac{\partial T}{\partial y} \right|. \tag{9.12}$$

Eq. (9.12) implies that baroclinic storm generation depends on the existence and magnitude of meridional temperature differences and the static stability of the midlatitude atmosphere. According to Eq. (9.12), any processes that enhance the static stability of the midlatitude atmosphere would act to suppress baroclinic storm generation, whereas any processes that enhance the meridional temperature gradient would act to promote baroclinic storm generation. This theoretical framework will be used as the basis for understanding the interactions between clouds and the midlatitude circulation discussed in this section. Results from recent studies of both observations and model simulations will be examined.

9.3.1 Influence of the midlatitude circulation on cloud properties

Baroclinic storms propagate preferentially within the midlatitude storm track regions of the North Atlantic, North Pacific, and Southern Oceans, so at planetary scales, midlatitude cloud and radiation changes can result either from a) changes in the location of those storm track regions or b) from changes in the strength or frequency of the individual baroclinic storms.

9.3.1.1 Changes in storm track position

The positions of the baroclinic storm tracks at both Northern and Southern Hemisphere midlatitudes are not static in time, but rather fluctuate between more poleward and more equatorward positions on the timescale of approximately 10 days. These modes of unforced variability in the extratropical atmospheric flow are referred to as the Northern and Southern Annular Modes, respectively. The exact dynamics that govern the annular modes are still being researched. In brief, from Eq. (9.12), the maximum growth rates of baroclinic eddies occur where the meridional temperature gradients are largest. The baroclinic eddies formed at the latitude of the maximum meridional temperature gradient act to flux momentum back toward their formation region, driving a region of enhanced westerly winds from the surface to the upper troposphere called the eddy-driven jet stream. Consequently, if the location of the strongest meridional temperature gradient is perturbed poleward or equatorward, the baroclinic storm tracks and eddy-driven jet stream will closely follow. The momentum fluxes by the baroclinic waves are thought to be crucial in maintaining the storm track and eddy-driven jet stream in a more poleward or equatorward position for 1–2 weeks (Lorenz and Hartmann, 2001).

The latitudinal shifts in the baroclinic storm tracks and eddy-driven jet stream associated with the annular modes should be accompanied by corresponding cloud property shifts, particularly in the high cloud field, as the intense upward motions in individual baroclinic storms should closely follow the location of the storm tracks and jet stream. In addition, the cloud shifts should be associated with coherent changes in the cloud radiative effects. Poleward storm track shifts are also sometimes linked to increases in midlatitude storm strength, but this may be due to the lower climatological sea level pressure closer to the poles which makes a storm shift appear as an increase in the SLP-defined storm strength even if the storm circulation is not stronger.

Analyses of both observational data gathered over the last 35 years and of model simulations can be used to examine the relationships between eddy-driven jet shifts and cloud properties. High clouds, for the most part, tend to shift consistently with the eddy-driven jets in most ocean basins and seasons. The high cloud shifts produce distinct longwave atmospheric warming in the region of increased high cloud cover (i.e., the latitudes toward which the jet and storm tracks have moved) and cooling in the region of reduced high cloud cover (i.e., the latitudes from which the jet and storm tracks have moved). Changes in the shortwave cloud radiative effects with eddy-driven jet shifts, however, are more complicated because low-top clouds do not respond in a systematic manner to eddy-driven jet shifts. The response of low-top clouds to eddy-driven jet shifts varies widely by ocean basin and often differs between observational data and model simulations (Grise and Medeiros, 2016).

In the North Atlantic, the poleward movement of the eddy-driven jet stream during the winter season produces a shortwave warming effect in areas equatorward of the jet, caused by a reduction in the total cloud amount in those areas that allows more sunlight to reach the ocean surface. The North Atlantic high cloud and cloud radiative effect changes are illustrated in Fig. 9.7, which shows the changes in high cloud amount (top panel), longwave cloud radiative effect (middle panel) and shortwave cloud radiative effect (bottom panel) for a one-degree poleward shift in the North Atlantic jet during winter. The high cloud amount shows a dipole change, with increases of 1–2% in the northern part of the basin and decreases of similar magnitude in the southern part of the basin, while the longwave cloud radiative effect change shows a corresponding warming of 1–2 $\mathrm{W\,m^{-2}}$ in the northern part of the basin and a cooling of 1–3 $\mathrm{W\,m^{-2}}$ in the southern part of the basin. The shortwave cloud radiative effect change shows mainly a 1–3 $\mathrm{W\,m^{-2}}$ warming in the southern part of the basin, since in the northern part of the basin, solar insolation is very small during the winter and therefore cloud changes do not produce a significant shortwave radiative signature.

In contrast to the North Atlantic winter season, in the summertime Northern Hemisphere and in all seasons in the Southern Hemisphere, a poleward eddy-driven jet shift produces a small shortwave cloud radiative cooling anomaly at the poleward part of the midlatitude domain ($\sim 50^\circ$ to 60° latitude) and does not produce any observable shortwave cloud radiative warming anomaly equatorward of the jet position. Understanding these complicated signatures is an area of active research, as they are not represented well in many present-day global climate models. The shortwave cooling at higher latitudes is likely produced through an increase in the liquid water path of the storm cloud field. The lack of shortwave warming equatorward of the jet shift is likely due to the presence of large amounts of low-top clouds in the lower midlatitude areas ($\sim 30^\circ$ to 45° latitude) of these ocean basins, and these clouds do not appear to respond in a co-

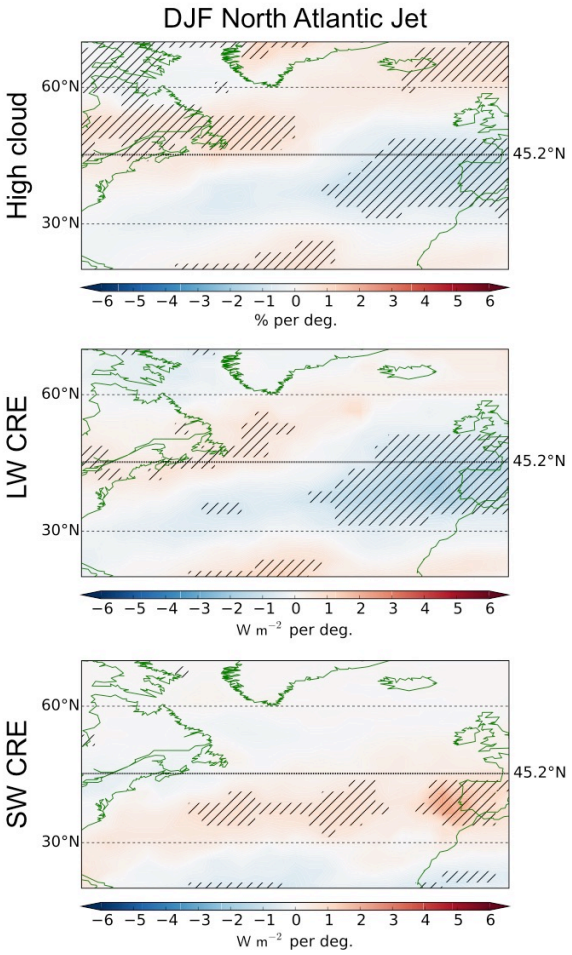

Figure 9.7 Changes in (top) high cloud amount, (middle) longwave cloud radiative effect (LW CRE) and (bottom) shortwave cloud radiative effect (SW CRE) for a one-degree poleward shift of the eddy-driven jet during winter over the North Atlantic ocean. The high cloud changes are shown in percentage units and the radiation changes in $\mathrm{W\,m^{-2}}$. Shaded regions denote statistically significant changes and the thicker horizontal line shows the mean position of the eddy-driven jet for that region and season. Adapted from Tselioudis et al. (2016). Copyright © 2016 John Wiley & Sons, Inc.

herent manner to eddy-driven jet shifts. As a matter of fact, a poleward movement of the eddy-driven jet is often correlated with a poleward expansion of the subsiding branch of the Hadley circulation, which creates favourable conditions for the formation of more extensive low cloud decks at the equatorward side of the midlatitude zones. Such increases in low clouds would negate the radiative effects of any decreases in the high cloud field with the poleward storm track shift. Consequently, variability of the midlatitude circulation and its effect on the midlatitude cloud field cannot be examined in isolation from the variability of the large-scale tropical circulation.

9.3.1.2 Changes in strength and frequency of baroclinic storms

Changes in midlatitude clouds and their radiative properties are also expected with changes in the strength and frequency of individual baroclinic storms. From Eq. (9.12), recall that the growth rates of baroclinic storms are closely related to the strength of the meridional temperature gradient and to the atmospheric stability, with more unstable lapse rates promoting greater baroclinic eddy growth. As illustrated in Fig. 9.4, the amount of high cloud in baroclinic storms depends strongly on storm strength changes and, to a lesser extent, on the moisture availability of the atmospheric column. Table 9.1 quantifies the changes in cloud radiative effect associated with changes in midlatitude storm strength and frequency, as derived from observations. The values in Table 9.1 represent the shortwave and longwave cloud radiative effect responses to a 7% decrease in the overall midlatitude storm frequency and to a 5% increase in overall storm intensity. These changes in frequency and intensity were used because they represent typical values occurring in climate warming simulations (see Section 9.4 for further discussion of climate change impacts on midlatitude clouds).

The results in Table 9.1 show that changes in storm strength and frequency have opposite effects on cloud radiative effects. Storm strength increases produce shortwave cooling and longwave warming through the production of optically thicker clouds with higher cloud tops. These cloud changes occur in the cold and warm frontal sections of the storms as shown in Fig. 9.4. The shortwave cooling is of order 2–5 $\mathrm{W\,m^{-2}}$, depending on hemisphere and season, and the longwave warming is of order 1.5–2.5 $\mathrm{W\,m^{-2}}$. As a result, a 5% increase in storm strength results in a net cooling of order 1.5 $\mathrm{W\,m^{-2}}$. It must be noted again, however, that shortwave cooling materialises at Earth's surface while longwave warming materialises in the tropospheric column, and therefore the shortwave and longwave effects affect fundamentally different processes in the Earth system.

Storm frequency decreases, on the other hand, produce shortwave warming and longwave cooling through an overall decrease in the amount, optical depth, and height of the cloud field. The shortwave warming is of order 1.5–2.5 $\mathrm{W\,m^{-2}}$ and the longwave cooling is of order 0.5–1.5 $\mathrm{W\,m^{-2}}$. As a result, a 7% decrease in storm frequency results in a net warming of order 1 $\mathrm{W\,m^{-2}}$. It is clear that the net cloud radiative effect of any combined storm strength and frequency change depends on the relative magnitude of change of the two dynamic components and the hemisphere and season where they occur. For this particular storm change configuration, the overall radiative change is dominated by the shortwave cooling caused by the storm strength increase. Note that the magnitudes of the radiative signatures from these relatively modest changes in storm strength and frequency are of order 1–5 $\mathrm{W\,m^{-2}}$, implying the potential for strong radiative effects from climate perturbations in the characteristics of baroclinic storms.

		Winter		Summer	
		SW	LW	SW	LW
Northern Hemisphere	Increasing storm strength	-3.7	+1.5	-1.9	+1.6
	Decreasing storm frequency	+2.6	-1.4	+1.9	-1.0
	Net change	-1.1	+0.1	0.0	+0.6
Southern Hemisphere	Increasing storm strength	-4.9	+2.5	-3.7	+1.4
	Decreasing storm frequency	+1.4	-0.3	+1.9	-0.4
	Net change	-3.5	+2.2	-1.8	+1.0

Table 9.1. *Net TOA shortwave (SW) and longwave (LW) flux changes in* $\mathrm{W\,m^{-2}}$ *with storm strength and frequency over midlatitude bands (*$30^\circ N$–$65^\circ N$ *and* $30^\circ S$–$65^\circ S$*) for winter and summer seasons. Adapted from Tselioudis and Rossow (2006).*

9.3.2 Influence of clouds on the midlatitude circulation

Unlike the tropics where diabatic processes are the key driver of the atmospheric circulation, the midlatitude circulation is governed more strongly by the presence of large horizontal temperature gradients. As discussed above, the location and strength of the eddy-driven jet streams and storm tracks depend on the thermal structure of the midlatitude atmosphere, and midlatitude clouds apply thermal forcings to the atmospheric column, both through radiative and latent heating effects. Differential thermal forcing by the clouds can produce horizontal and vertical temperature gradients that in turn could influence the midlatitude circulation, including the eddy-driven westerly jets. This forcing can happen at different spatial scales ranging from the global and climate scales to the local and synoptic scales. The Eady growth rate equation (9.12) indicates that storm growth responds to both temperature gradients and static stability changes, and both of those processes can be induced by changes in the structure and the properties of the midlatitude cloud field.

Clouds produce atmospheric thermal gradients either through the release of latent heat via condensation or through their interactions with atmospheric radiation. At the synoptic scale, emphasis has been put on the release of latent heat because the cloud-induced radiative heating is generally smaller by an order of magnitude than latent heating, and because observations of cloud-modified radiative fluxes have been sparse and less reliable. At such synoptic and local scales, cloud diabatic effects can damp or amplify the in-atmosphere energy balance of atmospheric eddies depending on whether the passage of storm clouds tends to warm an otherwise warm atmosphere or to warm an otherwise cold atmosphere. The cloud diabatic effects often depend on latitude and season as well as on the vertical distribution of the diabatic heating.

Modelling and observational studies generally show that latent heat release leads to stronger storms and faster storm development. In the vertically tilted structure of a baroclinic storm, the latent heat release associated with cloudy air ascending the frontal structure of the warm conveyor belt is often accompanied by evaporative cooling from precipitation falling into the dry air intrusion behind the cold front (Fig. 9.2). This creates a heating dipole along the front that increases baroclinicity, which could strengthen the storm circulation. Despite their relatively smaller magnitude, radiative heating terms could also play a role in affecting baroclinic storm development. As discussed in Section 9.2, shortwave cloud radiative cooling effects tend to dampen the surface horizontal temperature gradients in low pressure systems, while longwave cloud warming effects tend to strengthen the upper tropospheric horizontal temperature gradients. In addition, longwave cooling that peaks above the cloud top combined with longwave warming below can create vertical diabatic heating gradients especially near the tropopause, which can induce circulations that ~~strengthen~~ the amplitude of the baroclinic storm. It is difficult to observe diabatic heating rates with sufficient spatial and temporal resolutions to resolve interactions between clouds and synoptic-scale dynamics. However, modelling analyses indicate that latent heat release is an important contributor to the storm energy budget at the early stages of high latitude winter storms (Booth et al., 2013), while radiative effects could play an important role in the development of high latitude summertime storms when shortwave effects are the strongest. It is fair to say that we are still at the beginning stages of understanding the interactions between cloud-scale thermodynamic processes and synoptic-scale midlatitude weather systems.

On global climate scales, the radiative effects of midlatitude clouds, particularly the effects on shortwave radiation, are generally considered to be the most important diabatic cloud effects on the midlatitude circulation. Shortwave cloud radiative effects cool the surface and therefore modulate horizontal temperature gradients and surface baroclinicity, particularly during the summer season when the solar insolation at midlatitudes is maximised. The existence of bands of strong shortwave cloud radiative forcing over the midlatitude storm tracks introduces an additional cooling component that sharpens the meridional temperature gradient on the equatorward side of the midlatitude storm tracks, which affects the baroclinicity (see Eq. (9.12)) and could therefore subsequently feed back upon the strength and location of the eddy-driven jets and storm tracks. The strength of this shortwave cloud radiative forcing depends on the cloud amount and the optical depth of the midlatitude cloud field. It is important to also note, however, that the existence of shortwave cloud radiative cooling at middle latitudes decreases meridional temperature gradients on the poleward side of mid-

latitude ocean basins and therefore can decrease the baroclinicity in higher latitude regions. Therefore, the shortwave radiative effects of midlatitude clouds depend strongly on the mean position of the storm tracks.

Studies of the radiative effects of midlatitude clouds on the large-scale midlatitude circulation are done mostly in the context of atmospheric models, often run in idealised frameworks such as the aqua-planet framework in which the Earth's surface is entirely ocean. Such modelling studies suggest that cloud changes that favour increases in the gradient of absorbed shortwave radiation between high and low latitudes increase midlatitude baroclinicity and produce a poleward shift and a strengthening of the eddy-driven jet streams (Ceppi and Hartmann, 2016). Model simulations also suggest that cloud radiative effects within the atmosphere, achieved mostly through longwave absorption in the atmospheric column, exhibit important influences on the large-scale circulation. Model sensitivity experiments demonstrate that these in-atmosphere radiative effects strengthen the eddy-driven jet stream and increase eddy kinetic energy by as much as 30% (Li et al., 2015). This effect is achieved through an increase of the in-atmosphere meridional temperature gradient and decreases in static stability in the midlatitude upper troposphere.

The modelling results point to a strong dependence of the midlatitude circulation on cloud radiative effects. It must be noted, however, that atmospheric models include in their simulations strong biases in their midlatitude radiative budgets, manifested in most models through a strong positive bias in absorbed shortwave radiation at middle and high latitudes (Trenberth and Fasullo, 2010). This is due to the fact that most climate models simulate a midlatitude cloud field that includes too few yet too optically thick clouds. Models simulate high, optically thick cloud decks along the warm conveyor belt circulations of midlatitude storms. However, for the most part, they fail to simulate the extensive middle and low cloud decks that occur in the cold air outbreak regimes that follow the passage of the frontal structures (Bodas-Salcedo et al., 2014). These cold air outbreak regimes are associated with large-scale subsidence, so the failure of models to accurately simulate low cloud decks here is consistent with their similar struggles in the subsiding regimes of the tropics and subtropics (Chapter 8). As a result, most climate models allow excess amounts of shortwave radiation to reach the midlatitude surface and at the same time misrepresent the horizontal radiative gradients that exist between the different sectors of baroclinic storms, which are important factors in the storms' development. The existence of these cloud errors and radiative biases make the results of model studies of midlatitude cloud/dynamics interactions difficult to interpret and motivates the need for stricter observational constraints.

9.4 Midlatitude clouds in a changing climate

The midlatitude cloud systems discussed in this Chapter are likely to be significantly altered over the coming century (see also Chapter 13). With increasing greenhouse gas concentrations, the troposphere is expected to warm and the stratosphere is expected to cool, which will raise the height of the global tropopause. A rising tropopause height will allow high-topped clouds to extend to higher altitudes at midlatitudes, increasing their longwave radiative warming capacity. However, because many midlatitude clouds are composed in part of ice, a warming troposphere will also promote the existence of more in-cloud liquid, increasing the optical depth of these clouds and consequently their shortwave radiative cooling capacity. Furthermore, as the troposphere warms, the saturation vapour pressure will increase exponentially with temperature via the Clausius-Clapeyron relationship (~~Eq. (10.1).~~ Fig. 2.1), and thus there will be increased moisture availability for midlatitude clouds and the energetics of midlatitude storms. Absolute humidity gradients are also projected to increase, which would make mixing more effective in stabilising saturated regions.

The changing climate will also likely alter midlatitude circulation patterns. Global climate models suggest that, with increasing greenhouse gas concentrations, the storm tracks and eddy-driven jet streams will shift poleward, particularly in the Southern Hemisphere. The mechanisms for these poleward jet and storm track shifts are not well understood. Several leading hypotheses rely on the fact that, in a warming climate, upper tropospheric temperatures will increase substantially more than surface temperatures, particularly in the tropics and subtropics. The large warming of the tropical upper troposphere (compared to that at the surface) is due to the fact that the tropical atmospheric lapse rate is approximately moist adiabatic . Greater warming in the subtropical and midlatitude upper troposphere would enhance the static stability on the equatorward side of the present-day storm track, acting to suppress baroclinic eddy growth there (see Eq. (9.12)) and thus promoting a poleward shift of the storm track (Vallis et al., 2015). Because warming of the tropical upper troposphere strengthens the meridional temperature gradient in the upper troposphere-lower stratosphere, the enhanced meridional temperature gradient in the upper troposphere-lower stratosphere might also be a critical component in driving the poleward shift in the storm track and eddy-driven jet. A complicating factor is that, as the climate warms, enhanced warming of the Arctic surface ~~due to ice-albedo feedbacks~~ ("polar amplification") will act to reduce the surface pole-to-equator temperature gradient in the Northern Hemisphere, which has been shown to promote an equatorward shift in the storm tracks and eddy-driven jet stream in model experiments (Butler et al., 2010).

Regardless of the mechanism involved, systematic poleward jet and storm track shifts are likely to have fundamental impacts on midlatitude cloud fields (as noted in Section 9.3.1.1). Some recent satellite observations suggest that midlatitude cloud fields have already begun to shift poleward (Bender et al., 2012). Recent observed poleward jet and storm track shifts are more pronounced in the Southern Hemisphere and can be attributed, at least in part, to the existence of the Antarctic ozone hole, which is thought to have contributed to a pronounced poleward jet and storm track shift in the Southern Hemisphere summer months since

the early 1980s. The ozone hole is associated with substantial cooling in the Southern Hemisphere polar lower stratosphere during spring and summer months, which enhances the meridional temperature gradient in the upper troposphere-lower stratosphere. Antarctic polar stratospheric ozone levels are expected to recover by the mid to late 21st century, so the Southern Hemisphere summertime storm tracks would be expected to return to a more equatorward position by the mid-21st century in the absence of increasing greenhouse gases.

The strength and frequency of individual midlatitude storms is also likely to be impacted by the changing climate. Enhanced warming in the upper troposphere compared to that at the surface would increase midlatitude static stability, which would have a weakening effect on storm intensity via Eq. (9.12). Likewise, enhanced warming of the Arctic surface would act to reduce the surface pole-to-equator temperature gradient in the Northern Hemisphere, reducing the surface baroclinicity available for the growth of baroclinic storms. However, the predicted increase in atmospheric moisture content and the upper tropospheric-lower stratospheric temperature gradient might be expected to increase the strength of baroclinic storms. There is little consensus about whether baroclinic storms will increase or decrease in strength in a warming climate, while there is some agreement among climate models that baroclinic storms will reduce in frequency, particularly in the Northern Hemisphere (Chang et al., 2012). As noted in the introduction to this ../CHAPTER, the purpose of baroclinic storms is to transport energy from equator to pole. If the equator-to-pole temperature gradient is reduced, the amount of required energy transport would be reduced. Similarly, if the amount of moisture in baroclinic storms increases, weaker storms could attain the same required energy transport. From these simple arguments, fewer or weaker storms might be expected in a warmer climate. Systematic changes in storm magnitude and frequency will have fundamental impacts on midlatitude cloud fields and their radiative impacts, as noted in Section 9.3.1.2.

Midlatitude cloud changes induced directly by warming temperatures or indirectly through midlatitude circulation changes can potentially feed back on the position and strength of the atmospheric circulation via changes in horizontal and vertical temperature gradients in diabatic heating (as discussed in Section 9.3.2). It remains an area of active research as to how much midlatitude clouds and their responses to a changing climate will impact future changes in baroclinic storms and the large-scale midlatitude circulation.

Exercises

1. Using $\boldsymbol{v_g} = (1/\boldsymbol{f_0}) \times \nabla_p \phi$, show that the rhs of Eq. (9.1) is equivalent to the rhs of Eq. (9.4). Make the quasi-geostrophic Beta plane approximation.

2. Show that the thermodynamic equation for a dry atmosphere (Eq. 9.5) can be rewritten in terms of the dry potential temperature θ (Eq. 2.46) as Eq. (9.6).

3. Show that the quasi-geostrophic vorticity equation (Eq. 9.8) can be derived from the quasi-geostrophic horizontal momentum equations (Eq. 9.4).

4. Show that the quasi-geostrophic omega equation (Eq. 9.9) can be derived from the quasi-geostrophic thermodynamic equation (Eq. 9.7) and vorticity equation (Eq. 9.8).

5. Explain why the Laplacian operator can be approximated as a negative sign in the interpretation of the quasi-geostrophic omega equation (Eq. 9.9).

6. Using your knowledge of the quasi-geostrophic omega equation (Eq. 9.9), draw a sketch of a typical midlatitude cyclone (as in Figs. 9.1 and 9.2). Label where the thermal advection, differential vorticity advection, and diabatic heating terms are likely to contribute to upward or downward motion.

7. The average daily solar insolation reaching the top of Earth's atmosphere is given by the following formula (see Hartmann (2016) for details):

$$\frac{S_0}{\pi}\left(\frac{\bar{d}}{d}\right)^2 [h_0 \sin\phi \sin\delta + \cos\phi \cos\delta \sin h_0], \qquad (9.13)$$

where $S_0 = 1360\,\mathrm{W\,m^{-2}}$ is the solar constant at Earth, $\bar{d} = 1.496 \times 10^{11}\,\mathrm{m} = 1$ AU is the mean earth-sun distance, d is the earth-sun distance, ϕ is latitude, and δ is the solar declination angle (the latitude at which the sun is directly overhead at noon, which varies from $-23.45°$ to $23.45°$). h_0 is the hour angle at sunrise and sunset (in radians), which is defined by $\cos h_0 = -\tan\phi \tan\delta$.

Using this formula, estimate the variation in solar insolation between the summer and winter solstices at 45°N and 45°S. The earth-sun distance on December 21 is 0.98376 AU, and the earth-sun distance on June 20 is 1.01618 AU.

8. Assuming a hydrostatic atmosphere (Eq. 2.136), derive the thermal wind relationship (Eq. 9.11) from the definition of the geostrophic wind (9.3). *Hint: You can assume that* $\boldsymbol{v_g}\frac{\mathrm{d}(\ln T)}{\mathrm{d}z}$ *is small and can be neglected.*

9. Using reanalysis data, plot the annual-mean climatology of the maximum Eady growth rate in the latitude-height plane. Explain the observed features within the context of the climatologies of the meridional temperature gradient and static stability.

10. Speculate on how increasing high and low cloud cover at midlatitudes may affect the midlatitude circulation. Justify your answer using the thermal wind equation (Eq. 9.11) and the Eady growth rate equation (Eq. 9.12).

Further Reading

This Chapter provided an overview of a wide range of extratropical cloud issues, related to their properties, their formation mechanisms, and their interaction with radiation and with atmospheric dynamics. Each of those issues is examined in more detail in the resources listed below.

Section 9.1: Midlatitude cloud structures

Carlson, *Mid-Latitude Weather Systems* (Carlson, 1998) This book provides a detailed discussion of the observed structures and dynamics in extratropical cyclones from a synoptic meteorology perspective. Topics covered include the Norwegian cyclone model, baroclinic storm development, and quasi-geostrophic theory.

Cotton, Bryan and Van den Heever, *Storm and Cloud Dynamics* (Cotton et al., 2010) This book provides extensive coverage of the relationships between cloud formations and dynamical circulations across a range of mesoscale and synoptic-scale weather systems. Their Chapter 10 includes further detail on the relationships between clouds and dynamics in extratropical cyclones.

Holton and Hakim, *An Introduction to Dynamic Meteorology* (Holton and Hakim, 2013) This book provides a detailed introduction to atmospheric dynamics, ranging from fundamental concepts such as geostrophic and thermal wind balance to more advanced topics on the atmospheric general circulation. Their ../CHAPTERs 6 and 7 provide further detail on quasi-geostrophic theory and baroclinic instability, respectively.

Section 9.3: Interaction of clouds with the midlatitude circulation

Ceppi and Hartmann, *Connections between clouds, radiation, and midlatitude dynamics: A review* (Ceppi and Hartmann, 2015) This short review article provides an overview of the recent scientific literature linking variability in midlatitude dynamics with clouds and their associated radiative feedbacks.

Section 9.4: Midlatitude clouds in a changing climate

Shaw et al., *Storm track processes and the opposing influences of climate change* (Shaw et al., 2016) This review article provides a detailed summary of the recent scientific literature on the dynamics of baroclinic storm tracks, their linkages with moist processes, and processes relevant for explaining their changes in a warming climate.

REFERENCES

Abercromby, R. 1888. Cloud-land in folk-lore and in science. *The Folk-Lore Journal*.

Ackerman, A.S., Kirkpatrick, M.P., Stevens, D.E., and Toon, O.B. 2004. The impact of humidity above stratiform clouds on indirect aerosol cli- mate forcing. *Nature*, **432**, 1014–1017.

Ackerman, Thomas P., and Stokes, Gerald M. 2003. The Atmospheric Radiation Measurement Program. *Physics Today*, **56**(1), 38.

Adams, J. 2010. *Vegetation-Climate interaction, how plants make the global environment*. Springer.

Allan, Richard P., Liu, Chunlei, Zahn, Matthias, Lavers, David A., Koukouvagias, Evgenios, and Bodas-Salcedo, Alejandro. 2014. Physically Consistent Responses of the Global Atmospheric Hydrological Cycle in Models and Observations. *Surveys in Geophysics*, **35**(3), 533–552.

Andrews, Timothy, Gregory, Jonathan M., Webb, Mark J., and Taylor, Karl E. 2012. Forcing, feedbacks and climate sensitivity in CMIP5 coupled atmosphere-ocean climate models. *Geophys. Res. Lett.*, **39**(9). L09712.

Arakawa, A. 1969. Parameterization of cumulus convection. Pages 1–6 of: *Proc. WMO/IUGG Symp. Numerical Weather Prediction*.

Arakawa, A., and Schubert, H. 1974. Interaction of a cumulus cloud ensemble with the large-scale environment. Part I. Theoretical formulation and sensitivity tests. *J. Atmos. Sci.*, **31**, 674–701.

Arakawa, Akio. 2004. The Cumulus Parameterization Problem: Past, Present, and Future. *Journal of Climate*, **17**(13), 2493–2525.

Arakawa, Akio, and Wu, Chien-Ming. 2013. A Unified Representation of Deep Moist Convection in Numerical Modeling of the Atmosphere. Part I. *Journal of the Atmospheric Sciences*, **70**(7), 1977–1992.

Arora, V. 2002. Modeling vegetation as a dynamic component in soil-vegetation-atmosphere transfer schemes and hydrological models. *Reviews of Geophysics*, **40**, 1–26.

Arrhenius, S. 1896. On the Influence of Carbonic Acid in the Air upon the Temperature of the Ground. *Philosophical Magazine and Journal of Science*, **41**, 237–276.

Asai, T., and Kasahara, A. 1967. A Theoretical Study of the Compensating Downward Motions Associated with Cumulus Clouds. *J. Atmos. Sci.*, **24**, 467–496.

Augstein, E., Riehl, Herbert, Ostapoff, F., and Wagner, V. 1973. Mass and Energy Transports in an Undisturbed Atlantic Trade-Wind flow. *Monthly Weather Review*, **101**(2), 101–111.

Bailey, M., and Hallett, J. 2009. A Comprehensive Habit Diagram for Atmospheric Ice Crystals: Confirmation from the Laboratory, AIRS II, and Other Field Studies. *J. Atmos. Sci*, **66**.

Bannon, P R. 2002. Theoretical foundations for models of moist convection. *Journal of the Atmospheric Sciences*, **59**(12), 1967–1982.

Barenblatt, G I. 1996. *Scaling, self similarity, and intermediate asymptotics*. Cambridge, UK: Cambridge University Press.

Bauer, M. P., Tselioudis, G., and Rossow, W. B. 2016. A new climatology for investigating storm influences in and on the extratropics. *J. Appl. Meteorol. Climatol.*, **55**, 1287–1303.

Beard, K. V. 1977. Terminal Velocity Adjustment for Cloud and Precipitation Drops Aloft. *J. Atmos. Sci*, **34**, 1293–1298.

Bellon, G., and Sobel, A. H. 2010. Multiple equilibria of the Hadley circulation in an intermediate-complexity axisymmetric model. *J. Climate*, **23**, 1760–1778.

Bellouin, N., Jones, A., Haywood, J., and Christopher, S. A. 2008. Updated estimate of aerosol direct radiative forcing from satellite observations and comparison against the Hadley Centre climate model. *J. Geophys. Res.*, **113**, D10205.

Bellouin, N., Quaas, J., Morcrette, J.-J., and Boucher, O. 2013. Estimates of aerosol radiative forcing from the MACC reanalysis. *Atmos. Chem. Phys.*, **13**, 2045–2062.

Bender, F. A-M., Ramanathan, V., and Tselioudis, G. 2012. Changes in extratropical storm track cloudiness 1983–2008: Observational support for a poleward shift. *Climate Dyn.*, **38**, 2037–2053.

Betts, A. K., and Ridgway, W. 1988. Coupling of the radiative, convective, and surface fluxes over the Equatorial Pacific. *J. Atmos. Sci.*, **45**(3), 522–536.

Betts, A. K., and Ridgway, W. 1989. Climatic equilibrium of the atmospheric convective boundary layer over a tropical ocean. *J. Atmos. Sci.*, **46**(17), 2621–2641.

Bjerknes, J., and Solberg, H. 1922. Life cycle of cyclones and the polar front theory of atmospheric circulation. *Geophysisks Publikationer*, **3**, 3–18.

Bjerknes, Jakob. 1969. Atmospheric teleconnections from the equatorial Pacific. *Monthly Weather Review*, **97**(3), 163–172.

Bodas-Salcedo, A., Webb, M. J., Bony, S., Chepfer, H., Dufresne, J.-L., Klein, S. A., Zhang, Y., Marchand, R., Haynes, J M, Pincus, R., and John, V O. 2011. COSP: Satellite simulation software for model assessment. *Bulletin of the American Meteorological Society*, **92**(8), 1023–1043.

Bodas-Salcedo, A., Williams, K. D., Field, P. R., and Lock, A. P. 2012. The Surface Downwelling Solar Radiation Surplus over the Southern Ocean in the Met Office Model: The Role of Midlatitude Cyclone Clouds. *Journal of Climate*, **25**(21), 7467–7486.

Bodas-Salcedo, A., Williams, K. D., Ringer, M. A., Beau, I., Cole, J. N. S., Dufresne, J.-L., Koshiro, T., Stevens, B., Wang, Z., and Yokohata, T. 2014. Origins of the solar radiation biases over the Southern Ocean in CFMIP2 models. *J. Climate*, **27**, 41âĂŞ–56.

Boers, R., de Haij, M. J., Wauben, W. M. F., Baltink, H. Klein, van Ulft, L. H., Savenije, M., and Long, C. N. 2010. Optimized fractional cloudiness determination from five ground-based remote sensing techniques. *Journal of Geophysical Research*, **115**(D24), D24116.

Bohren, Craig F. 1987. Multiple scattering of light and some of its observable consequences. *American Journal of Physics*, **55**(6), 524–533.

Bohren, Craig F., and Clothiaux, Eugene E. 2006. *Fundamentals of Atmospheric Radiation*. John Wiley and Sons.

Boing, S.J., Siebesma, A.P, Korpershoek, J.D., and Jonker, Harm J.J. 2012. Detrainment in Deep Convection. *Geophys. Res. Lett.*, **39**, 20–30.

Böing, Steven J, Jonker, Harm J J, Nawara, Witek A, and Siebesma, A Pier. 2014. On the Deceiving Aspects of Mixing Diagrams of Deep Cumulus Convection. *J. Atmos. Sci*, **71**(1), 56–68.

Bollasina, M., Ming, Y., and Ramaswamy, V. 2011. Anthropogenic aerosols and the weakening of the South Asian summer monsoon. *Science*, **334**, 502–505.

Bolton, David. 1980. The Computation of Equivalent Potential Temperature. *Mon Weather Rev*, **108**(7), 1046–1053.

Bony, S., Dufresne, J.-L., Le Treut, H., Morcrette, J.-J., and Senior, C. 2004. On dynamic and thermodynamic components of cloud changes. *Clim. Dyn.*, **22**(2-3), doi:10.1007–s00382–003–0369–6.

Bony, S., Stevens, B., Held, I., Mitchell, J., Dufresne, J.-L., Emanuel, K., Friedlingstein, P., Griffies, S., and Senior, C. 2013a. *Carbon Dioxide and climate: Perspectives on a scientific assessment*. Vol. Monograph on Climate Science for Serving Society: Research, Modeling and Prediction Priorities. Springer. Pages 391–413.

Bony, Sandrine, Colman, Robert, Kattsov, Vladimir M, Allan, Richard P, Bretherton, Christopher S, Dufresne, Jean-Louis, Hall, Alex, Hallegatte, Stephane, Holland, Marika M, Ingram, William, Randall, David A, Soden, Brian J, Tselioudis, George, and Webb, Mark J. 2006. How Well Do We Understand and Evaluate Climate Change Feedback Processes? *J. Climate*, **19**(15), 3445–3482.

Bony, Sandrine, Stevens, Bjorn, Held, Isaac H, Mitchell, John F, Dufresne, Jean-Louis, Emanuel, Kerry A, Friedlingstein, Pierre, Griffies, Stephen, and Senior, Catherine. 2013. *Carbon Dioxide and Climate: Perspectives on a Scientific Assessment*. Springer. Pages 391–413.

Bony, Sandrine, Bellon, Gilles, Klocke, Daniel, Sherwood, Steven, Fermepin, Solange, and Denvil, Sebastien. 2013b. Robust direct effect of carbon dioxide on tropical circulation and regional precipitation. *Nature Geosci.*, **6**(6), 447–451.

Bony, Sandrine, Stevens, Bjorn, Frierson, Dargan M W, Jakob, Christian, Kageyama, Masa, Pincus, Robert, Shepherd, Theodore G, Sherwood, Steven C, Siebesma, A Pier, Sobel, Adam H, Watanabe, Masahiro, and Webb, Mark J. 2015. Clouds, circulation and climate sensitivity. *Nature Geosci*, **8**(4), 261–268.

Bony, Sandrine, Stevens, Bjorn, Coppin, David, Becker, Tobias, Reed, Kevin A., Voigt, Aiko, and Medeiros, Brian. 2016. Thermodynamic control of anvil cloud amount. *Proc. Nat. Acad. Sci.*, **113**(32), 8927–8932.

Booth, B.B.B., Dunstone, N.J., Halloran, P.R., Andrews, T., and Bellouin, N. 2012. Aerosols implicated as a prime driver of twentieth-century North Atlantic climate variability. *Nature*, **484**, 228–232.

Booth, J. F., Wang, S., and Polvani, L. M. 2013. Midlatitude storms in a moister world: lessons from idealized baroclinic life cycle experiments. *Climate Dyn.*, **41**, 787âĂŞ–802.

Boucher, O. 2015. *Atmospheric Aerosols - Properties and Climate Impacts*. Dordrecht: Springer.

Boucher, O, Randall, D, Artaxo, P, Bretherton, C, Feingold, G, Forster, P, Kerminen, V-M, Kondo, Y, Liao, H, Lohmann, U, Rasch, P, Satheesh, S K, Sherwood, S, Stevens, B, and Zhang, X Y. 2013. Clouds and Aerosols. Chap. 7, pages 571–657 of: *Climate Change 2013: The Physical Science Basis*. Cambridge University Press.

Boutle, I. A., Eyre, J. E. J., and Lock, A. P. 2014. Seamless Stratocumulus Simulation across the Turbulent Gray Zone. *Monthly Weather Review*, **142**(4), 1655–1668.

Bras, R. L. 1990. *Hydrology: An introduction to hydrologic science*. Addison-Wesley.

Bretherton, C. S., and Wyant, M. C. 1997. Moisture transport, lower-tropospheric stability, and decoupling of cloud-topped boundary layers. *J. Atmos. Sci.*, **54**, 148–167.

Bretherton, C. S., Blossey, P. N., and Khairoutdinov, M. 2005. An energy-balance analysis of deep convective self-aggregation above uniform SST. *J. Atmos. Sci.*, **62**, 4273–4292.

Bretherton, C. S., Blossey, P. N., and Uchida, J. 2007. Cloud droplet sedimentation, entrainment efficiency, and subtropical stratocumulus albedo. *Geophys. Res. Lett.*, **34**.

Bretherton, Christopher S. 2015. Insights into low-latitude cloud feedbacks from high-resolution models. *Phil. Trans. Roy. Soc. A*, **373**(2054).

Bretherton, Christopher S., and Park, Sungsu. 2009. A New Moist Turbulence Parameterization in the Community Atmosphere Model. *Journal of Climate*, **22**(12), 3422–3448.

Brient, Florent, and Bony, Sandrine. 2013. Interpretation of the positive low-cloud feedback predicted by a climate model under global warming. *Climate Dynamics.*, **40**, 2415–2431.

Brooks, C.E.P. 1927. The mean cloudiness over the earth. *Mem. r. meteor. Soc.*, **1**(10), 127–138.

Butler, A. H., Thompson, D. W. J., and Heikes, R. 2010. The steady-state atmospheric circulation response to climate change-like thermal forcings in a simple general circulation model. *J. Climate*, **23**, 3274âĂŞ–3496.

Byers, H. R., and Braham Jr., R. R. 1949. *The thunderstorm: final report of the Thunderstorm project*. Washington, DC: U.S. Government Printing Office.

Caldwell, P., Zhang, Y., and Klein, S. 2013. CMIP3 subtropical stratocumulus cloud feedback interpreted through a mixed-layer model. *J. Clim.*, **26**, 1607–1625.

Callen, Herbert B. 1985. *Thermodynamics, and an Introduction to Thermostatics*. John Wiley & Sons inc.

Capderou, Michel. 2014. *Handbook of Satellite Orbits: From Kepler to GPS*. Springer.

Carlson, T. N. 1998. *Mid-Latitude Weather Systems*. American Meteorological Society, xx+507 pp.

Ceppi, P., and Hartmann, D. L. 2015. Connections between clouds, radiation, and midlatitude dynamics: A review. *Curr. Clim. Change Rep.*, **1**, 94–102.

Ceppi, P., and Hartmann, D. L. 2016. Clouds and the atmospheric circulation response to warming. *J. Climate*, **29**, 783âĂŞ–799.

Ceppi, Paulo, Brient, Florent, Zelinka, Mark D., and Hartmann, Dennis L. 2017. Cloud feedback mechanisms and their representation in global climate models. *Wiley Interdisciplinary Reviews: Climate Change*, **8**(4), e465. e465.

Cesana, G., Kay, J. E., Chepfer, H., English, J. M., and de Boer, G. 2012. Ubiquitous low-level liquid-containing Arctic

clouds: New observations and climate model constraints from CALIPSO-GOCCP. *Geophysical Research Letters*, **39**(20), n/a–n/a. L20804.

Cess, R. D. 1976. Climate change: an appraisal of atmospheric feedback mechanisms employing zonal climatology. *J. Atmos. Sci.*, **33**(10), 1831–1843.

Cess, R. D., Potter, G. L., Blanchet, J. P., Boer, G. J., Del Genio, A. D., DÃľquÃľ, M., Dymnikov, V., Galin, V., Gates, W. L., Ghan, S. J., Kiehl, J. T., Lacis, A. A., Le Treut, H., Li, Z.-X., Liang, X.-Z., McAvaney, B. J., Meleshko, V. P., Mitchell, J. F. B., Morcrette, J.-J., Randall, D. A., Rikus, L., Roeckner, E., Royer, J. F., Schlese, U., Sheinin, D. A., Slingo, A., Sokolov, A. P., Taylor, K. E., Washington, W. M., Wetherald, R. T., Yagai, I., and Zhang, M.-H. 1990. Intercomparison and interpretation of climate feedback processes in 19 atmospheric general circulation models. *J. Geophys. Res.*, **95**(D10), 16601–16615.

Chang, E. K. M., Y., Guo, and X., Xia. 2012. CMIP5 multimodel ensemble projection of storm track change under global warming. *J. Geophys. Res. Atmos.*, **117**, D23118, doi:10.1029/2012JD018578.

Charlson, R., Lovelock, J., Andreae, M., and Warren, S. 1987. Oceanic phytoplankton, atmospheric sulphur, cloud albedo and climate. *Nature*, **326**, 655–661.

Charney, J. G. 1963. A note on large-scale motions in the tropics. *J. Atmos. Sci.*, **20**(6), 607–609.

Charney, J. G. 1979. Carbon Dioxide and climate: a scientific assessment. *National Academy Press, 33pp.*

Chen, Yi-Chun, Christensen, Matthew W, Stephens, Graeme L, and Seinfeld, John H. 2014. Satellite-based estimate of global aerosol-cloud radiative forcing by marine warm clouds. *Nature Geosci*, **7**(9), 643–646.

Cherian, R., Quaas, J., Salzmann, M., and Wild, M. 2014. Pollution trends over Europe constrain global aerosol forcing as simulated by climate models. *Geophys. Res. Lett.*, **41**, 2176–2181.

Chou, Chia, and Neelin, J. David. 2004. Mechanisms of Global Warming Impacts on Regional Tropical Precipitation. *J. Climate*, **17**(13), 2688–2701.

Christensen, M.W., Suzuki, K., Zambri, B., and Stephens, G.L. 2014. Ship track observations of a reduced shortwave aerosol indirect effect in mixed-phase clouds. *Geophys. Res. Lett.*, **41**, 6970–6977.

Clarke, Allan J. 2008. *An introduction to the dynamics of El Niño and the Southern Oscillation*. Academic press.

Claussen, M., Dallmeyer, A., and Bader, J. 2017. Theory and modeling of the African Humid Period and the Green Sahara. In: *Oxford Research Encyclopedias, climate science, regional and local climates, climate change*. DOI:10.1093/acrefore/9780190228620.013.532.

Connolly, P. J., Möhler, O., Field, P. R., Saathoff, H., Burgess, R., Choularton, T., and Gallagher, M. 2009. Studies of heterogeneous freezing by three different desert dust samples. *Atmos. Chem. Phys*, **9**, 2805–2824.

Conover, J.H. 1966. Anomalous cloud lines. *J. Atmos. Sci.*, **23**, 778–785.

Cotton, W.R., Bryan, G., and Van den Heever, S. 2010. *Storm and Cloud Dynamics, 2nd Edition*. Vol. 99. Academic Press.

Cox, P. M., Huntingford, C., and Williamson, M. S. 2018. Emergent constraint on equilibrium climate sensitivity from global temperature variability. *Nature*, **553**, 319.

Cronin, T. W., and Jansen, M. F. 2016. Analytic radiative-advective equilibrium as a model for high-latitude climate. *Geophys. Res. Lett.*, **43**(1), 449–457.

Cronin, T. W., and Tziperman, E. 2015. Low clouds suppress Arctic air formation and amplify high-latitude continental winter warming. *Proc. Nat. Acad. Sci.*, **112**(37).

Crosman, E. T., and Horel, J. D. 2010. Sea and Lake Breezes: A review of numerical studies. *Boundary-layer meteorology*, **137**, 1–29.

Curry, J. A., and Webster, P. J. 1999. *Thermodynamics of Atmospheres & Oceans*. Academic Press.

Curry, Judith. 1983. On the Formation of Continental Polar Air. *Journal of the Atmospheric Sciences*, **40**(9), 2278–2292.

Dal Gesso, S., and Neggers, R.A.J. 2017. Can we use single-column models for understanding the boundary-layer cloud-climate feedback? *J. Adv. Model. Earth Syst.*

David Randall. 2012. *Atmosphere, Clouds and Climate*. Princeton University Press.

Dawe, J.T., and Austin, P.H. 2011. Interpolation of LES cloud surfaces for use in direct calculations of entrainment and detrainment. *Mon. Wea. Rev.*, **139**, 444–456.

De Roode, S. R., and Duynkerke, P. G. 1997. Observed Lagrangian transition of stratocumulus into cumulus during ASTEX: Mean state and turbulence structure. *J. Atmos. Sci.*, **54**, 2157–2173.

De Roode, S. R., Duynkerke, P. G., and Jonker, H. J. J. 2004. Large Eddy Simulation: How large is large enough? *J. Atmos. Sci.*, **61**, 403–421.

De Roode, S. R., Siebesma, A. P., Dal Gesso, S., Jonker, H. J. J., Schalkwijk, J., and Sival, J. 2014. A mixed-layer model study of the stratocumulus response to changes in large-scale conditions. *J. Adv. Model. Earth Syst.*, **6**(4), 1256–1270.

De Roode, S. R, Sandu, I., van der Dussen, J. J., Ackerman, A. S., Blossey, P., Jarecka, D., Lock, A., Siebesma, A. P., and Stevens, B. 2016. Large eddy simulations of EUCLIPSE/GASS Lagrangian stratocumulus to cumulus transitions: Mean state, turbulence, and decoupling. *J. Atmos. Sci.*, **73**, 2485–2508.

de Roode, S.R., Siebesma, A.P., Jonker, H.J.J., and de Voogd, Y. 2012. Parameterization of the Vertical Velocity Equation for Shallow Cumulus Clouds. *Mon. Wea. Rev.*, **140**, 2424–2436.

de Rooy, Wim C., and Siebesma, A. Pier. 2008. A Simple Parameterization for Detrainment in Shallow Cumulus. *Monthly Weather Review*, **136**(2), 560–576.

de Rooy, Wim C., Bechtold, Peter, FrÃűhlich, Kristina, Hohenegger, Cathy, Jonker, Harm, Mironov, Dmitrii, Pier Siebesma, A., Teixeira, Joao, and Yano, Jun-Ichi. 2013. Entrainment and detrainment in cumulus convection: an overview. *Quarterly Journal of the Royal Meteorological Society*, **139**(670), 1–19.

Delworth, T. L., and Manabe, S. 1988. The influence of potential evaporation on the variabilities of simulated soil wetness and climate. *Journal of Climate*, **1**, 523–547.

Diaz, Henry F, and Bradley, Raymond S. 2004. *The Hadley circulation: present, past, and future*. Springer.

Dirmeyer, P. A., and Brubaker, K. L. 2007. Characterization of the global hydrologic cycle from a back-trajectory analysis of atmospheric water vapor. *Journal of hydrometeorology*, **8**, 20–37.

Dorrestijn, Jesse, Crommelin, Daan T., Siebesma, A. Pier, Jonker, Harmen J. J., and Selten, Frank. 2016. Stochastic Convection Parameterization with Markov Chains in an Intermediate-Complexity GCM. *Journal of the Atmospheric Sciences*, **73**(3), 1367–1382.

Dufresne, Jean-Louis, and Bony, Sandrine. 2008. An Assessment of the Primary Sources of Spread of Global Warming Esti-

mates from Coupled Atmosphere–Ocean Models. *Journal of Climate*, **21**(19), 5135–5144.

Dufresne, Jean-Louis, and Saint-Lu, Marion. 2016. Positive Feedback in Climate: Stabilization or Runaway, Illustrated by a Simple Experiment. *Bull. Amer. Meteorol. Soc.*, **97**(5), 755–765.

Dunstone, N. J., Smith, D. M., Booth, B. B. B., Hermanson, L., and Eade, R. 2013. Anthropogenic aerosol forcing of Atlantic tropical storms. *Nature Geosci.*, **6**, 534–539.

Durant, A. J., and Shaw, A. 2005. Evaporation freezing by contact nucleation inside-out. *Geophysical Research Letters*, **32**.

Duynkerke, P. G., , Zhang, H.-Q., and Jonker, P. J. 1995. Microphysical and turbulent structure of nocturnal stratocumulus as observed during ASTEX. *J. Atmos. Sci.*, **52**, 2763–2777.

Duynkerke, P. G., de Roode, S. R., van Zanten, M. C., Calvo, J., Cuxart, J., Cheinet, S., Chlond, A., Grenier, H., Jonker, P. J., Köhler, M., Lenderink, G., Lewellen, D., Lappen, C.-L., Lock, A. P., Moeng, C.-H., Müller, F., Olmeda, D., Piriou, J.-M., Sanchez, E., and Sednev, I. 2004. Observations and numerical simulations of the diurnal cycle of the EUROCS stratocumulus case. *Quart. J. Roy. Meteorol. Soc.*, **130**, 3269–3296.

Ek, M., and Mahrt, L. 1994. Daytime evolution of relative humidity at the boundary layer top. *Monthly Weather Review*, **122**, 2709–2721.

Emanuel, K.. 1994. *Atmospheric Convection*. Oxford University Press.

Emanuel, Kerry. 2003. Tropical Cyclones. *Annual Review of Earth and Planetary Sciences*, **31**(1), 75–104.

Faloona, I., Lenschow, D. H., Campos, T., Stevens, B., Zanten, M. Van, Blomquist, B., Thornton, D., Bandy, A., and Gerber, H. 2005. Observations of entrainment in eastern Pacific marine stratocumulus using three conserved scalars. *J. Atmos. Sci.*, **62**, 3268–3285.

Fang, Ming, and Tung, Ka Kit. 1996. A simple model of nonlinear Hadley circulation with an ITCZ: Analytic and numerical solutions. *Journal of the atmospheric sciences*, **53**(9), 1241–1261.

Feng, Y., and Ramanathan, V. 2010. Investigation of aerosol-cloud interactions using a chemical transport model constrained by satellite observations. *Tellus*, **62B**, 69–86.

Fermi, E. 1956. *Thermodynamics*. Dover Publications.

Field, P. R., and Wood, R. 2007. Precipitation and cloud structure in midlatitude cyclones. *J. Climate*, **20**, 233–254.

Field, P. R., J., Heymsfield A., A., Bansemer, and Twohy, C. H. 2008. Determination of the combined ventilation factor and capacitance for ice crystal aggregates from airborne observations in a tropical anvil cloud. *J. Atmos. Sci*, **65**, 376–391.

Findell, K. L., and Eltahir, E. A. B. 2003. Atmospheric controls on soil moisture-boundary layer interactions. Part I: Framework development. *Journal of hydrometeorology*, **4**, 552–569.

Fischer, E. M., Seneviratne, S. I., Vidale, P. L., Lüthi, D., and Schär, C. 2007. Soil moisture-atmosphere interactions during the 2003 European summer heat wave. *Journal of Climate*, **20**, 5081–5099.

Flato, G. M., Marotzke, J., Abiodun, B, Braconnot, P., Chou, S C, Collins, W., Cox, P, Driouech, F, Emori, S., Eyring, V., Forest, Chris E., Glecker, Peter J., Guilyardi, E., Jakob, C, Kattsov, V. M., Reason, C, and Rummukainen, M. 2013. Evaluation of Climate Models. Pages 741–866 of: on Climate Change, Intergovernmental Panel (ed), *Climate Change 2013 - The Physical Science Basis*. Cambridge: Cambridge University Press.

Forster, Piers M. 2016. Inference of Climate Sensitivity from Analysis of Earth's Energy Budget. *Annual Review of Earth and Planetary Sciences*, **44**(1), 85–106.

Freud, E., and Rosenfeld, D. 2012. Linear relation between convective cloud drop number concentration and depth for rain initiation. *J. Geophys. Res.*, **117**, D02207.

Frisch, Uriel. 1996. *Turbulence, the Legacy of A. N. Kolmogorov*. Cambridge: Cambridge University Press.

Garcia-Herrera, R., Diaz, J., Trigo, R. M., Luterbacher, J., and Fischer, E. M. 2010. A review of the European summer heat wave of 2003. *Critical Reviews in Environmental Science and Technology*, **40**, 267–306.

Geoffroy, O, Saint-Martin, D, Olivié, D J L, Voldoire, A, Bellon, G, and Tyteca, S. 2013. Transient Climate Response in a Two-Layer Energy-Balance Model. Part I: Analytical Solution and Parameter Calibration Using CMIP5 AOGCM Experiments. *J. Climate*, **26**(6), 1841–1857.

Gerst, Alexander. 2017. *Astro Alex*. `https://www.flickr.com/photos/astro_alex/`. Accessed: 2017-01-15.

Gill, Adrian E. 1980. Some simple solutions for heat-induced tropical circulation. *Quarterly Journal of the Royal Meteorological Society*, **106**(449), 447–462.

Gill, Adrian E. 1982. *Atmosphere-ocean Dynamics*. Elsevier.

Gleckler, P. J., Taylor, K. E., and Doutriaux, C. 2008. Performance metrics for climate models. *J. Geophys. Res.*, **113**(D6), D06104.

Golaz, Jean-Christophe, Larson, Vincent E., and Cotton, William R. 2002. A PDF-Based Model for Boundary Layer Clouds. Part I: Method and Model Description. *Journal of the Atmospheric Sciences*, **59**(24), 3540–3551.

Gordon, Neil D., and Klein, Stephen A. 2014. Low-cloud optical depth feedback in climate models. *J. Geophys. Res.*, **119**(10), 6052–6065.

Goren, T., and Rosenfeld, D. 2014. Decomposing aerosol cloud radiative effects into cloud cover, liquid water path and Twomey components in marine stratocumulus. *Atmos. Res.*, **138**, 378–393.

Govekar, Pallavi D, Jakob, Christian, and Catto, Jennifer. 2014. The relationship between clouds and dynamics in Southern Hemisphere extratropical cyclones in the real world and a climate model. *Journal of Geophysical Research: Atmospheres*, **119**(11), 6609–6628.

Grabowski, W. W., and Wang, L. P. 2013. Growth of Cloud Droplets in a Turbulent Environment. *Annu. Rev. Fluid Mech*, **45**, 293–324.

Grabowski, Wojciech W, and Smolarkiewicz, Piotr K. 1999. CRCP: a Cloud Resolving Convection Parameterization for modeling the tropical convecting atmosphere. *Physica D: Nonlinear Phenomena*, **133**(1), 171 – 178.

Grant, A. L. M., and Brown, A. R. 1999. A similarity hypothesis for shallow-cumulus transports. *Quarterly Journal of the Royal Meteorological Society*, **125**(558), 1913–1936.

Gregory, J. M., Ingram, W. J., Palmer, M. A., Jones, G. S., Stott, P. A., Thorpe, R. B., Lowe, J. A., Johns, T. C., and Williams, K. D. 2004. A new method for diagnosing radiative forcing and climate sensitivity. *Geophys. Res. Lett.*, **31**(3). L03205.

Gregory, Jonathan M, Andrews, Timothy, and Good, Peter. 2015. The inconstancy of the transient climate response parameter under increasing CO_2. *Phil. Trans. Roy. Soc. A*, July, 1–25.

Grise, K. M., and Medeiros, B. 2016. Understanding the varied influence of midlatitude jet position on clouds and cloud radiative effects in observations and global climate models. *J. Climate*, **29**, 9005aĂŞ–9025.

Gunn, R., and Kinzer, G. D. 1949. The terminal velocity of fall for water droplets in stagnant air. *J. Meteor*, **6**, 243–248.

Hagemann, S. 2002. *An improved land surface parameter dataset for global and regional climate models*. Max Planck Institute for Meteorology Report No 336.

Hagos, Samson, Zhang, Chidong, Tao, Wei-Kuo, Lang, Steve, Takayabu, Yukari N., Shige, Shoichi, Katsumata, Masaki, Olson, Bill, and L'Ecuyer, Tristan. 2010. Estimates of tropical diabatic heating profiles: commonalities and uncertainties. *Journal of Climate*, **23**(3), 542–558.

Hahn, C. J., and Warren, S.G. 2007. *A Gridded Climatology of Clouds over Land (1971-96) and Ocean (1954-97) from Surface Observations Worldwide*. Numeric Data Package NDP-026E. CDIAC, Department of Energy, Oak Ridge, Tennessee.

Halley, E. 1686. An historical account of the trade winds and monsoons, observable in the seas between and near the tropicks, with an attempt to assign the physical cause of the said winds. *Philosophical Transactions of the Royal Society*, **16**, 153–168.

Hartmann, Dennis. 2016. *Global Physical Climatology, 2nd Edition*. Elsevier Science.

Hartmann, Dennis L., and Larson, Kristin. 2002. An important constraint on tropical cloud - climate feedback. *Geophysical Research Letters*, **29**(20), 12–1–12–4. 1951.

Haynes, John M., Jakob, Christian, Rossow, William B., Tselioudis, George, and Brown, Josephine. 2011. Major Characteristics of Southern Ocean Cloud Regimes and Their Effects on the Energy Budget. *Journal of Climate*, **24**(19), 5061–5080.

Hazeleger, W., and coauthors. 2010. EC-Earth, A Seamless Earth-System Prediction Approach in Action. *Bull. Amer. Meteor. Soc.*, **91**, 1357–1363.

Held, Isaac M, and Hou, Arthur Y. 1980. Nonlinear axially symmetric circulations in a nearly inviscid atmosphere. *Journal of the Atmospheric Sciences*, **37**(3), 515–533.

Held, Isaac M., and Soden, Brian J. 2006. Robust Responses of the Hydrological Cycle to Global Warming. *J. Climate*, **19**(21), 5686–5699.

Hogan, Robin J., and Illingworth, Anthony J. 2000. Deriving cloud overlap statistics from radar. *Quarterly Journal of the Royal Meteorological Society*, **126**(569), 2903–2909.

Hogstrom, U. 1996. Review of Some Basic Characteristics of the Atmospheric Surface Layer. *Boundary Layer Meteorology*, **78**, 215–246.

Hohenegger, C., Brockhaus, P., Bretherton, C. S., and Schär, C. 2009. The soil moisture-precipitation feedback in simulations with explicit and parameterized convection. *Journal of Climate*, **22**, 5003–5020.

Holton, J. R., and Hakim, G. J. 2013. *An Introduction to Dynamic Meteorology*. Fifth edn. Academic Press, xvi+532 pp.

Holtslag, A.A.M., and Duynkerke, P.G. 1998. *Clear and Cloudy Boundary Layers: Proceedings of the Colloquium "Clear and Cloudy Boundary Layers," Amsterdam, 26-29 August 1997*. Verhandelingen der Koninklijke Nederlandse Akademie van Wetenschappen, Afd. Natuurkunde: Eerste reeks. Royal Netherlands Academy of Arts and Sciences.

Hoskins, B. J., and Hodges, K. I. 2002. New perspectives on the Northern Hemisphere winter storm tracks. *J. Atmos. Sci.*, **59**, 1041âĂŞ–1061.

Hourdin, Frederic, Mauritsen, Thorsten, Gettelman, Andrew, Golaz, Jean-Christophe, Balaji, Venkatramani, Duan, Qingyun, Folini, Doris, Ji, Duoying, Klocke, Daniel, Qian, Yun, Rauser, Florian, Rio, Catherine, Tomassini, Lorenzo, Watanabe, Masahiro, and Williamson, Daniel. 2017. The Art and Science of Climate Model Tuning. *Bulletin of the American Meteorological Society*, **98**(3), 589–602.

Houze, Jr., R. A., and Betts, A. K. 1981. Convection in GATE. *Reviews of Geophysics and Space Physics*, **19**(Nov.), 541–576.

Houze, Robert. 1993. *Cloud Dynamics*. Vol. 53. Academic Press.

Houze, Robert A. 2004. Mesoscale convective systems. *Reviews of Geophysics*, **42**(4).

Howell, Wallace E. 1949. The growth of cloud drops in uniformly cooled air. *Journal of Meteorology*, **6**(2), 134–149.

Hughes, N.A. 1984. Global cloud climatologies: a historical review. *Journal of Applied Meteorology and Climatology*, **23**, 724–751.

Iribarne, J V, and Godson, W L. 1981. *Atmospheric Thermodynamics*. Holland: Dordrecht.

Jakob, Christian, and Tselioudis, George. 2003. Objective identification of cloud regimes in the Tropical Western Pacific. *Geophysical Research Letters*, **30**(21), 2082, doi: 10.1029/2003GL018367–doi: 10.1029–2003GL018367.

Jiang, Jonathan H., Su, Hui, Zhai, Chengxing, Perun, Vincent S, Del Genio, Anthony, Nazarenko, Larissa S, Donner, Leo J., Horowitz, Larry, Seman, Charles, Cole, Jason, Gettelman, Andrew, Ringer, Mark A, Rotstayn, Leon, Jeffrey, Stephen, Wu, Tongwen, Brient, Florent, Dufresne, Jean-Louis, Kawai, Hideaki, Koshiro, Tsuyoshi, Watanabe, Masahiro, L'Ecuyer, Tristan S., Volodin, Evgeny M, Iversen, Trond, Drange, Helge, Mesquita, Michel d.S., Read, William G, Waters, Joe W, Tian, Baijun, Teixeira, Joao, and Stephens, Graeme L. 2012. Evaluation of cloud and water vapor simulations in CMIP5 climate models using NASA "A-Train" satellite observations. *J. Geophys. Res.*, **117**(D14), D14105.

Johnson, Richard H, Rickenbach, Thomas M, Rutledge, Steven A, Ciesielski, Paul E, and Schubert, Wayne H. 1999. Trimodal characteristics of tropical convection. *Journal of climate*, **12**(8), 2397–2418.

Kahn, B. H., Teixeira, J., Fetzer, E. J., Gettelman, A., Hristova-Veleva, S. M., Huang, X., Kochanski, A. K., KÃűhler, M., Krueger, S. K., Wood, R., and Zhao, M. 2011. Temperature and Water Vapor Variance Scaling in Global Models: Comparisons to Satellite and Aircraft Data. *Journal of the Atmospheric Sciences*, **68**(9), 2156–2168.

Kain, J.S., and Frisch, J.M. 1990. A one-dimensional entraining/detraining plume model and its application in convective parameterization. *J. Atmos. Sci.*, **479**, 2784–2802.

Kamae, Youichi, and Watanabe, Masahiro. 2013. Tropospheric adjustment to increasing CO2: its timescale and the role of land–sea contrast. *Climate Dynamics*, **41**(11), 3007–3024.

Kärcher, B., and Lohmann, U. 2003. A parameterization of cirrus cloud formation: Heterogeneous freezing. *J. Geophys. Res.*, **108**, 4402.

Karlsson, K.-G., and Dybbroe, A. 2010. Evaluation of Arctic cloud products from the EUMETSAT Climate Monitoring Satellite Application Facility based on CALIPSO-CALIOP observations. *Atmospheric Chemistry and Physics*, **10**(4), 1789–1807.

Kay, Jennifer E., L'Ecuyer, Tristan, Chepfer, Helene, Loeb, Norman, Morrison, Ariel, and Cesana, Gregory. 2016. Recent Advances in Arctic Cloud and Climate Research. *Current Climate Change Reports*, **2**(4), 159–169.

Kessler, E. 1995. On the continuity and distribution of water substance in atmospheric circulations. *Atmospheric Research*, **38**(1-4), 109–145.

Khouider, B., Biello, J., and Majda, A. J. 2010. A stochastic multicloud model for tropical convection. *Commun. Math. Sci.*, **8**(1), 187–216.

Khvorostyanov, V. I., and Curry, J. A. 2006. Aerosol size spectra and CCN activity spactra: Reconciling the lognormal, algebraic, and power lows. *J. Geophys. Res*, **111**, 148–0227.

Kiladis, George N, Wheeler, Matthew C, Haertel, Patrick T, Straub, Katherine H, and Roundy, Paul E. 2009. Convectively coupled equatorial waves. *Reviews of Geophysics*, **47**(2).

Kinne, S., O'Donnell, D., Stier, P., Kloster, S., Zhang, K., Schmidt, H., Rast, S., Giorgetta, M., Eck, T., and Stevens, B. 2013. MAC-v1: A new global aerosol climatology for climate studies. *J. Adv. Model. Earth Syst.*, **5**, 704–740.

Kleidon, A, and Renner, M. 2013. A simple explanation for the sensitivity of the hydrologic cycle to surface temperature and solar radiation and its implications for global climate change. *Earth Syst. Dynam.*, **4**(2), 455–465.

Klein, Rupert. 2010. Scale-dependent models for atmospheric flows. *Annu. Rev. Fluid Mech.*, **42**, 249–274.

Klein, S. A., and Jakob, C. 1999. Validation and sensitivities of frontal clouds simulated by the ECMWF model. *Monthly Weather Review*, **127**, 2514–2531.

Klein, Stephen A., Pincus, Robert, Hannay, Cecile, and Xu, Kuan-Man. 2005. How might a statistical cloud scheme be coupled to a mass-flux convection scheme? *Journal of Geophysical Research: Atmospheres*, **110**(D15), 10–15.

Klocke, Daniel, Pincus, Robert, and Quaas, Johannes. 2011. On Constraining Estimates of Climate Sensitivity with Present-Day Observations through Model Weighting. *Journal of Climate*, **24**(23), 6092–6099.

Knutti, Reto, and Sedláček, Jan. 2013. Robustness and uncertainties in the new CMIP5 climate model projections. *Nature Clim. Change*, **369**(3).

Koster, R. D., and Suarez, M. J. 2001. Soil moisture memory in climate models. *Journal of hydrometeorology*, **2**, 559–570.

Kuang, Zhiming. 2008. Modeling the interaction between cumulus convection and linear gravity waves using a limited-domain cloud system–resolving model. *Journal of the Atmospheric Sciences*, **65**(2), 576–591.

Kuhlmann, J., and Quaas, J. 2010. How can aerosols affect the Asian summer monsoon? Assessment during three consecutive pre-monsoon seasons from CALIPSO satellite data. *Atmos. Chem. Phys.*, **10**, 4673–4688.

Kulmala, M., T. Suni, Lehtinen, K.E.J., Maso, M. Dal, Boy, M., Reissell, A., Rannik, U., Aalto, P., Keronen, P., Hakola, H., Back, J., Homann, T., Vesala, T., and Hari, P. 2004. A new feedback mechanism linking forests, aerosols, and climate. *Atmos. Chem. Phys.*, **4**, 557–562.

Kundu, Pijush K, and Cohen, Ira M. 2002. *Fluid Mechanics*. 2nd edn. San Diego: Academic Press.

Lamarque, J.-F., Bond, T. C., Eyring, V., Granier, C., Heil, A., Klimont, Z., Lee, D., Liousse, C., Mieville, A., Owen, B., Schultz, M. G., Shindell, D., Smith, S. J., Stehfest, E., Van Aardenne, J., Cooper, O. R., Kainuma, M., Mahowald, N., McConnell, J. R., Naik, V., Riahi, K., and van Vuuren, D. P. 2010. Historical (1850–2000) gridded anthropogenic and biomass burning emissions of reactive gases and aerosols: Methodology and application. *Atmos. Chem. Phys.*, **10**, 7017–7039.

Lappen, Cara-Lyn, and Randall, David A. 2001. Toward a Unified Parameterization of the Boundary Layer and Moist Convection. Part I: A New Type of Mass-Flux Model. *Journal of the Atmospheric Sciences*, **58**(15), 2021–2036.

Lau, N.-C., and Crane, M. W. 1997. Comparing satellite and surface observations of cloud patterns in synoptic-scale circulation systems. *Mon. Wea. Rev.*, **125**, 3172–3189.

Lau, William K-M, and Waliser, Duane E. 2011. *Intraseasonal variability in the atmosphere-ocean climate system*. Springer.

L'Ecuyer, Tristan S., Beaudoing, H. K., Rodell, M., Olson, W., Lin, B., Kato, S., Clayson, C. A., Wood, E., Sheffield, J., Adler, R., Huffman, G., Bosilovich, M., Gu, G., Robertson, F., Houser, P. R., Chambers, D., Famiglietti, J. S., Fetzer, E., Liu, W. T., Gao, X., Schlosser, C. A., Clark, E., Lettenmaier, D. P., and Hilburn, K. 2015. The Observed State of the Energy Budget in the Early Twenty-First Century. *Journal of Climate*, **28**(21), 8319–8346.

Lenderink, G., and Holtslag, A. A. M. 2000. Evaluation of the Kinetic Energy Approach for Modeling Turbulent Fluxesin Stratocumulus. *Monthly Weather Review*, **128**(1), 244–258.

Lenoble, Jacqueline. 1993. *Atmospheric Radiative Transfer*. Studies in Geophysical Optics and Remote Sensing. A Deepak Publishing.

Li, Ying, Thompson, David WJ, and Bony, Sandrine. 2015. The influence of atmospheric cloud radiative effects on the large-scale atmospheric circulation. *Journal of Climate*, **28**(18), 7263–7278.

Liepert, B., Feichter, J., Lohmann, U., and Roeckner, E. 2004. Can aerosols spin down the hydrological cycle in a moister and warmer world? *Geophy. Res. Lett.*, **31**, L06207.

Lindzen, R. S., and Farrell, B. 1980. A simple approximate result for the maximum growth rate of baroclinic instabilities. *J. Atmos. Sci.*, **37**, 1648–1654.

Loeb, N.G., and Wielicki, B.A. 2015. Earth's Radiation Budget. Pages 67 – 76 of: North, Gerald R., Pyle, John, and Zhang, Fuqing (eds), *Encyclopedia of Atmospheric Sciences (Second Edition)*. Academic Press.

Lohmann, U. 2002. A glaciation indirect aerosol effect caused by soot aerosols. *Geophys. Res. Lett.*, **29**, 1052.

Lohmann, U., and Feichter, J. 2005. Global indirect aerosol effects: a review. *Atmos. Chem. Phys.*, **5**, 715–737.

Lohmann, U., Quaas, J., Kinne, S., and Feichter, J. 2007. Different approaches for constraining global climate models of the anthropogenic indirect aerosol effect. *Bull. Amer. Meteor. Soc.*, **88**, 243–249.

Lohmann, U., Lüönd, F., and Mahrt, F. 2016. *An Introduction to Clouds from the microscale to climate*. Cambridge: Cambridge University Press.

Lorenz, D. J., and Hartmann, D. L. 2001. Eddy-zonal flow feedback in the Southern Hemisphere. *J. Atmos. Sci.*, **58**, 3312aĂŞ–3327.

Madden, Roland A, and Julian, Paul R. 1972. Description of global-scale circulation cells in the tropics with a 40–50 day period. *Journal of the atmospheric sciences*, **29**(6), 1109–1123.

Mahmood, R., Pielke Sr, R. A., Hubbard, K. G., Niyogi, D., Dirmeyer, P. A., McAlpine, C., Carleton, A. M., Hale, R., Gameda, S., Beltran-Przekurat, A., Baker, B., McNider, R., Legates, D. R., Shepherd, M., Du, J., Blanken, P. D., Frauenfeld, O. W., Nair, U. S., and Fall, S. 2014. Land cover changes and their biogeophysical effects on climate. *International Journal of climatology*, **34**, 929–953.

Malkus, J. S., Scorer, R.S., Ludlam, F.H., and Bjorgum, O. 1953. Correspondence - Bubble theory of penetrative convection. *Quart. J. Roy.Meteor.Soc.*, **79**, 288–293.

Malkus, Joanne, and Scorer, R S. 1955. The erosion of cumulus towers. *Journal of Meteorology*, **12**(1), 43–57.

Manabe, S., and Wetherald, R. T. 1967. Thermal equilibrium of the atmosphere with a given distribution of relative humidity. *J. Atmos. Sci.*, **24**(3), 241–259.

Manabe, S., Smagorinsky, J., and Strickler, R. F. 1965. Simulated climatology of a general circulation model with a hydrological cycle. *Monthly Weather Review*, **93**, 769–798.

Mapes, Brian, Tulich, Stefan, Lin, Jialin, and Zuidema, Paquita. 2006. The mesoscale convection life cycle: Building block or prototype for large-scale tropical waves? *Dynamics of atmospheres and oceans*, **42**(1), 3–29.

Martin, G. M., Johnson, D. W., and Spice, S. 1994. The measurement and parameterization of effective radius of droplets in warm stratocumulus clouds. *J. Atmos. Sci.*, **51**, 1823–1842.

Mason, B. J. 1971. The Physics of Clouds. *Clarendon Press, Oxford*, **671**.

Mason, Shannon, Fletcher, Jennifer K, Haynes, John M, Franklin, Charmaine, Protat, Alain, and Jakob, Christian. 2015. A Hybrid Cloud Regime Methodology Used to Evaluate Southern Ocean Cloud and Shortwave Radiation Errors in ACCESS. *J. Climate*, **28**(15), 6001–6018.

Matsuno, Taroh. 1966. Quasi-geostrophic motions in the equatorial area. *Journal of the Meteorological Society of Japan. Ser. II*, **44**(1), 25–43.

Mauritsen, T., Sedlar, J., Tjernström, M., Leck, C., Martin, M., Shupe, M., Sjogren, S., Sierau, B., Persson, P. O. G., Brooks, I. M., and Swietlicki, E. 2011. An Arctic CCN-limited cloud-aerosol regime. *Atmospheric Chemistry and Physics*, **11**(1), 165–173.

McDonald, J. E. 1963. Use of the electrostatic analogy in studies of ice crystal growth. *Z. Angew. Math. Phys*, **14**.

McDonald, James E. 1958. The Physics of Cloud Modification. *Advances in Geophysics*, **5**, 223–303.

Medeiros, Brian, and Stevens, Bjorn. 2011. Revealing differences in GCM representations of low clouds. *Climate Dynamics*, **36**(1), 385–399–399.

Mellado, Juan Pedro. 2010. The evaporatively driven cloud-top mixing layer. *Journal of Fluid Mechanics*, **660**(Oct.), 5–36.

Mellado, Juan Pedro. 2017. Cloud-Top Entrainment in Stratocumulus Clouds. *Annu. Rev. Fluid Mech.*, **49**(1), 145–169.

Mellor, George L. 1977. The Gaussian Cloud Model Relations. *Journal of the Atmospheric Sciences*, **34**(2), 356–358.

Ming, Y., Ramaswamy, V., and Persad, G. 2010. Two opposing effects of absorbing aerosols on global-mean precipitation. *Geophys. Res. Lett.*, **37**, L13701.

Mironov, Dmitrii V. 2008. *Turbulence in the lower troposphere: Second-order closure and mass-flux modelling frameworks.* Springer, Berlin, Heidelberg.

Mishchenko, Michael I., Hovenier, Joop W., and Travis, Larry D. (eds). 2000. *Light Scattering by Nonspherical Particles: Theory, Measurements, and Applications.* Academic Press.

Mitchell, D. L., and Heymsfield, A. J. 2005. Refinements in the Treatment of Ice Particle Terminal Velocities, Highlighting Aggregates. *J. Atmos. Sci*, **62**, 1637–1644.

Mitchell, J. F. B., Wilson, C. A., and Cunnington, W. M. 1987. On CO_2 climate sensitivity and model dependence of results. *Quart. J. Roy. Meteor. Soc.*, **113**(475), 293–322.

Möhler, O., Field, P. R., Connolly, P., Benz, S., Saathoff, H., Schnaiter, M., Wagner, R., and Cotton, R. 2006. Efficiency of the deposition mode ice nu-cleation on mineral dust particles. *Atmos. Chem. Phys.*, **6**, 3007–3021.

Morrison, Hugh, de Boer, Gijs, Feingold, Graham, Harrington, Jerry, Shupe, Matthew D., and Sulia, Kara. 2012. Resilience of persistent Arctic mixed-phase clouds. *Nature Geoscience*, **5**(1), 11–17.

Muller, Caroline J., and Held, Isaac M. 2012. Detailed Investigation of the Self-Aggregation of Convection in Cloud-Resolving Simulations. *Journal of the Atmospheric Sciences*, **69**(8), 2551–2565.

Murphy, D M, and Koop, T. 2005. Review of the vapour pressures of ice and supercooled water for atmospheric applications. *Q.J.R. Meteorol. Soc.*, **131**(608), 1539–1565.

Neelin, J. D., and Zeng, N. 2000. A quasi-equilibrium tropical circulation model-formulation. *J. Atmos. Sci.*, **57**(11), 1741–1766.

Neelin, J David, and Held, Isaac M. 1987. Modeling Tropical Convergence Based on the Moist Static Energy Budget. *Mon Weather Rev*, **115**(1), 3–12.

Neggers, R. A. J. 2015. Exploring bin-macrophysics models for moist convective transport and clouds. *Journal of Advances in Modeling Earth Systems*, **7**(4), 2079–2104.

Neggers, R. A. J., Neelin, J. D., and Stevens, B. 2007. Impact mechanisms of shallow cumulus convection on tropical climate dynamics. *J. Climate*, **20**(11), 2623–2642.

Nicholls, S., and Turton, J. D. 1986. An observational study of the structure of stratiform cloud sheets: Part II. Entrainment. *Quart. J. Roy. Meteorol. Soc.*, **112**, 461–480.

Norris, J., and Slingo, A. 2009. Trends in Observed Cloudiness and EarthĀŢ s Radiation Budget. Chap. 2 of: Heintzenberg, J, and Charlson, Robert J (eds), *Clouds in the perturbed climate system : their relationship to energy balance, atmospheric dynamics, and precipitation.* The MIT Press.

O'Gorman, Paul A., Allan, Richard P., Byrne, Michael P., and Previdi, Michael. 2012. Energetic Constraints on Precipitation Under Climate Change. *Surveys in Geophysics*, **33**(3), 585–608.

Otto, A., Otto, F.E.L., Boucher, O., Church, J., Hegerl, G., Forster, P. M., Gillett, N. P., Gregory, J., Johnson, G. C., Knutti, R., Lewis, N., Lohmann, U., Marotzke, J., Myhre, G., Shindell, D., Stevens, B., and Allen, M. R. 2013. Energy budget constraints on climate response. *Nature Geosci.*, **415**(6).

Oueslati, Boutheina, and Bellon, Gilles. 2015. The double ITCZ bias in CMIP5 models: interaction between SST, large-scale circulation and precipitation. *Climate dynamics*, **44**(3-4), 585–607.

Park, S., Leovy, C. B., and Rozendaal, M. A. 2004. A new heuristic Lagrangian marine boundary layer cloud model. *J. Atmos. Sci.*, **61**, 3002–3024.

Pauluis, O, and Held, I M. 2002a. Entropy budget of an atmosphere in radiative-convective equilibrium. Part I: Maximum work and frictional dissipation. *Journal of the Atmospheric Sciences*, **59**(2), 125–139.

Pauluis, O, and Held, I M. 2002b. Entropy budget of an atmosphere in radiative-convective equilibrium. Part II: Latent heat transport and moist processes . *Journal of the Atmospheric Sciences*, **59**(2), 140–149.

Pawlowska, H., Grabowski, W. W., and Brenguier, J.-L. 2006. Observations of the width of cloud droplet spectra in stratocumulus. *Geophys. Res. Lett.*, **33**, L19810.

Perovich, Don K., Andreas, E. L., Curry, J. A., Eiken, H., Fairall, C. W., Grenfell, T. C., Guest, P.S., Intrieri, J., Kadko, D., Lindsay, R. W., McPhee, M. G., Morison, J., Moritz, R. E., Paulson, C. A., Pegau, W. S., Persson, P.O.G., Pinkel, R., Richter-Menge, J. A., Stanton, T., Stern, H., Sturm, M., Tucker, W.B., and Uttal, T. 1999. Year on ice gives climate insights. *Eos, Transactions American Geophysical Union*, **80**(41), 481–486.

Persson, P. Ola G., Shupe, Matthew D., Perovich, Don, and Solomon, Amy. 2016. Linking atmospheric synoptic transport, cloud phase, surface energy fluxes, and sea-ice growth: observations of midwinter SHEBA conditions. *Climate Dynamics*, 1–24.

Peters, Karsten, Crueger, Traute, Jakob, Christian, and Mobis, Benjamin. 2017. Improved MJO-simulation in ECHAM6.3 by coupling a Stochastic Multicloud Model to the convection scheme. *Journal of Advances in Modeling Earth Systems*, **9**(1), 193–219.

Petters, M. D., and Kreidenweis, S. M. 2007. A single parameter representation of hygroscopic growth and cloud condensation nuclei activity. *Atmos. Chem. Phys*, **7**, 1961–1971.

Petty, Grant W. 2006. *A First Course in Atmospheric Radiation (2nd edition)*. Sundog Publishing.

Pierrehumbert, R. T. 1995. Thermostats, radiator fins, and the local runaway greenhouse. *J. Atmos. Sci.*, **52**(10), 1784–1806.

Pierrehumbert, R. T., and Yang, H. 1993. Global chaotic mixing on isentropic surfaces. *J. Atmos. Sci.*, **50**(15), 2462–2480.

Pincus, Robert, Batstone, Crispian P., Hofmann, Robert J. Patrick, Taylor, Karl E., and Glecker, Peter J. 2008. Evaluating the present-day simulation of clouds, precipitation, and radiation in climate models. *J. Geophys. Res.*, **113**(D14), D14209, doi:10.1029/2007jd009334–doi:10.1029–2007jd009334.

Pincus, Robert, Platnick, Steven, Ackerman, Steven A, Hemler, Richard S, and Patrick Hofmann, Robert J. 2012. Reconciling Simulated and Observed Views of Clouds: MODIS, ISCCP, and the Limits of Instrument Simulators. *J. Climate*, **25**(13), 4699–4720.

Pino, D., Vilà-Guerau de Arellano, J., and Duynkerke, P. G. 2003. The contribution of shear to the evolution of a convective boundary layer. *J. Atmos. Sci.*, **60**(16), 1913–1926.

Pithan, Felix, Medeiros, Brian, and Mauritsen, Thorsten. 2014. Mixed-phase clouds cause climate model biases in Arctic wintertime temperature inversions. *Climate Dynamics*, **43**(1), 289–303.

Plant, RS, and Craig, George C. 2008. A stochastic parameterization for deep convection based on equilibrium statistics. *J. Atmos. Sci.*, **65**(1), 87–105.

Pope, Stephen B. 2000. *Turbulent Flows*. Cambridge: Cambridge University Press.

Posselt, D. J., Stephens, G. L., and Miller, M. 2008. CloudSat: Adding a new dimension to a classical view of extratropical cyclones. *Bull. Amer. Meteor. Soc.*, **89**, 599–609.

Pruppacher, H.R., and Klett, J.D. 2010. *Microphysics of Clouds and Precipitation*. Atmospheric and Oceanographic Sciences Library. Springer Netherlands.

Quaas, J. 2015. Approaches to observe effects of anthropogenic aerosols on clouds and radiation. *Current Climate Change Reports*, **1**, 297–304.

Quaas, J., Bony, S., Collins, W. D., Donner, L., Illingworth, A. J., Jones, A., Lohmann, U., Satoh, M., Schwartz, S. E., Tao, W.-K., and Wood, R. 2009. *Current understanding and quantification of clouds in the changing climate system and strategies for reducing critical uncertainties*. MIT press, Cambridge. Pages 557–573.

Quaas, J., Stevens, B., Lohmann, U., and Stier, P. 2010. Interpreting the cloud cover - aerosol optical depth relationship found in satellite data using a general circulation model. *Atmos. Chem. Phys.*, **10**, 6129–6135.

Quaas, Johannes. 2012. Evaluating the ĂIJcritical relative humidityĂİ as a measure of subgrid-scale variability of humidity in general circulation model cloud cover parameterizations using satellite data. *Journal of Geophysical Research: Atmospheres*, **117**(D9).

Ramage, Colin S. 1971. *Monsoon Meteorology (International geophysics series; v. 15)*. Academic Press.

Ramanathan, V, Cess, R D, Harrison, E F, Minnis, P, Barkstrom, B R, Ahmad, E, and Hartmann, D. 1989. Cloud-Radiative Forcing and Climate: Results from the Earth Radiation Budget Experiment. *Science*, **243**(4887), 57–63.

Randall, D. A., Krueger, S. K., Bretherton, C. S., Curry, J. A., Duynkerke, P. G., Moncrieff, M., Ryan, B. F., Starr, D., Miller, M. J., Rossow, W. B., Tselioudis, G., and Wielicki, B. 2003. Confronting models with data - The GEWEX Cloud Systems Study. *Bulletin of the American Meteorological Society*, **84**, 455–469.

Randall, D.A. 2000. *General Circulation Model Development: Past, Present, and Future*. International Geophysics. Elsevier Science.

Randall, David, DeMott, Charlotte, Stan, Cristiana, Khairoutdinov, Marat, Benedict, James, McCrary, Rachel, Thayer-Calder, Katherine, and Branson, Mark. 2016. Simulations of the Tropical General Circulation with a Multiscale Global Model. *Meteorological Monographs*, **56**, 15.1–15.15.

Randall, David A. 1980. Conditional Instability of the First Kind Upside Downocument. *J. Atmos. Sci*, **37**, 125–130.

Randall, David A., Shao, Qingqiu, and Moeng, Chin-Hoh. 1992. A Second-Order Bulk Boundary-Layer Model. *Journal of the Atmospheric Sciences*, **49**(20), 1903–1923.

Raymond, David J, Sessions, Sharon L, Sobel, Adam H, and Fuchs, Željka. 2009. The mechanics of gross moist stability. *J. Adv. Model. Earth Syst.*, **2**(Aug.).

Rieck, M., Nuijens, L., and Stevens, B. 2012. Marine Boundary Layer Cloud Feedbacks in a Constant Relative Humidity Atmosphere. *J. Atmos. Sci.*, **69**(Aug.), 2538–2550.

Riehl, H. 1954. *Tropical meteorology*. McGraw-Hill.

Riehl, H., and Malkus, J. S. 1957. On the heat balance and maintenance of circulation in the trades. *Quart. J. Roy.Meteor.Soc.*, **83**, 21–29.

Riehl, H., and Malkus, J. S. 1958. On the heat balance in the equatorial trough zone. *Geophysica*, **6:3-4**, 503–537.

Riley, Emily M, Mapes, Brian E, and Tulich, Stefan N. 2011. Clouds associated with the Madden–Julian oscillation: A new perspective from CloudSat. *Journal of the Atmospheric Sciences*, **68**(12), 3032–3051.

Rogers, R. R., and Yau, M. K. 1996. A Short Course in Cloud Physics. *Butterworth Heinemann*, **290**.

Romps, D. 2010. A direct measurement of entrainment. *J. Atmos. Sci.*, **67**, 1908–1927.

Rosenfeld, D., Lohmann, U., Raga, G.B., O'Dowd, C.D., Kulmata, M., Reissell, A., and Andreae, M.O. 2008. Flood or drought: How do aerosols affect precipitation? *Science*, **321**, 1309–1313.

Rossow, W. B., and Schiffer, R.A. 1999. Advances in understanding clouds from ISCCP. *Bull. Amer. Meteor. Soc.*, **80**(11), 2261–2287.

Rotstayn, L.D., and Lohmann, U. 2002. Tropical rainfall trends and the indirect aerosol effect. *J. Climate*, **15**, 2103–2116.

Royal Society. 2009. *Geoengineering the climate - Science, governance and uncertainty*. RS Policy document.

Sakradzija, Mirjana, Seifert, Axel, and Heus, Thijs. 2015. Fluctuations in a quasi-stationary shallow cumulus cloud ensemble. *Nonlinear Process. Geophys.*, **22**(1), 65–85.

Sanchez-Lorenzo, A., Laux, P., Hendricks-Franssen, H.-J., Georgoulias, A. K., Calbó, J., Vogl, S., and Quaas, J. 2012. As-

sessing large-scale weekly cycles in meteorological variables: a review. *Atmos. Chem. Phys.*, **12**, 5755–5771.

SCEP Study of Critical Environmental Problems. 1970. *Man's impact on the global environment.* The MIT Press.

Schalkwijk, J., Jonker, H. J. J., and Siebesma, A. P. 2013. Simple solutions to steady-state cumulus regimes in the convective boundary layer. *J. Atmos. Sci.*, **70**, 3656–3672.

Schalkwijk, J., Jonker, H.J.J., Siebesma, A.P., and Van Meijgaard, E. 2015. Weather forecasting using GPU-based Large-Eddy Simulations. *Bull. Amer. Meteor. Soc.*, **96**, 715–723.

Schär, C., Vidale, P. L., Lüthi, D., Frei, C., Häberli, C., Liniger, M. A., and Appenzeller, C. 2004. The role of increasing temperature variability in European summer heatwaves. *Nature*, **427**, 332–336.

Schemann, Vera, Stevens, Bjorn, Grutzun, Verena, and Quaas, Johannes. 2013. Scale Dependency of Total Water Variance and Its Implication for Cloud Parameterizations. *Journal of the Atmospheric Sciences*, **70**(11), 3615–3630.

Schneider, S. H. 1972. Cloudiness as a global climate feedback mechanisms: the effects on the radiation balance and surface temperature of variations in cloudiness. *J. Atmos. Sci.*, **29**, 1413–1422.

Schneider, Tapio, and Sobel, Adam H. 2007. *The global circulation of the atmosphere.* Princeton University Press.

Schulz, J., Albert, P., Behr, H.-D., Caprion, D., Deneke, H., Dewitte, S., Dürr, B., Fuchs, P., Gratzki, A., Hechler, P., Hollmann, R., Johnston, S., Karlsson, K.-G., Manninen, T., Müller, R., Reuter, M., Riihelä, A., Roebeling, R., Selbach, N., Tetzlaff, A., Thomas, W., Werscheck, M., Wolters, E., and Zelenka, A. 2009. Operational climate monitoring from space: the EUMETSAT Satellite Application Facility on Climate Monitoring (CM-SAF). *Atmospheric Chemistry and Physics*, **9**(5), 1687–1709.

Schumacher, Courtney, Zhang, Minghua H., and Ciesielski, Paul E. 2007. Heating Structures of the TRMM Field Campaigns. *Journal of the Atmospheric Sciences*, **64**(7), 2593–2610.

Schwartz, S. E. 2012. Determination of Earth's transient and equilibrium climate sensitivities from observations over the twentieth century: Strong dependence on assumed forcing. *Surv. Geophys.*, **33**, 745–777.

Schwartz, Stephen E. 2011. Feedback and sensitivity in an electrical circuit: an analog for climate models. *Climatic Change*, **106**(2), 315–326.

Seneviratne, S. I., Nicholls, N., Easterling, D., Goodess, C. M., Kanae, S., Kossin, J., Luo, Y., Marengo, J., McInnes, K., Rahimi, M., Reichstein, M., Sorteberg, A., Vera, C., and Zhang, X. 2012. Changes in climate extremes and their impacts on the natural physical environment. Pages 109–230 of: *Managing the Risks of Extreme Events and Disasters to Advance Climate Change Adaptation. [Field, C. B., V. Barros, T. F. Stocker, D. Qin, D. J. Dokken, K. L. Ebi, M. D. Mastrandrea, K. J. Mach, G.-K. Plattner, S. K. Allen, M. Tignor, and P. M. Midgley (eds.)]. A Special Report of Working Groups I and II of the Intergovernmental Panel on Climate Change (IPCC).* Cambridge University Press, Cambridge, United Kingdom and New York, NY, USA.

Seneviratne, S. I., Wilhelm, M., Stanelle, T., van den Hurk, B., Hagemann, S., Berg, A., Cheruy, F., Higgins, M. E., Meier, A., Brovkin, V., Claussen, M., Ducharne, A., Dufresne, J.-L., Findell, K. L., Ghattas, J., Lawrence, D. M., Malyshev, S., Rummukainen, M., and Smith, B. 2013. Impact of soil moisture-climate feedbacks on CMIP5 projections: First results from the GLACE-CMIP5 experiment. *Geophysical Research Letters*, **40**, 5212–5217.

Shaw, T. A., Baldwin, M., Barnes, E. A., Caballero, R., Garfinkel, C. I., Hwang, Y.-T., Li, C., O'Gorman, P. A., Rivière, G., Simpson, I. R., and Voigt, A. 2016. Storm track processes and the opposing influences of climate change. *Nat. Geosci.*, **9**, 656–664.

Sherwood, Steven C., Bony, Sandrine, and Dufresne, Jean-Louis. 2014. Spread in model climate sensitivity traced to atmospheric convective mixing. *Nature*, **505**(37).

Sherwood, Steven C, Bony, Sandrine, Boucher, Olivier, Bretherton, Chris, Forster, Piers M, Gregory, Jonathan M, and Stevens, Bjorn. 2015. Adjustments in the Forcing-Feedback Framework for Understanding Climate Change. *Bull. Amer. Meteorol. Soc.*, **96**(2), 217–228.

Shupe, M. D., Persson, P. O. G., Brooks, I. M., Tjernström, M., Sedlar, J., Mauritsen, T., Sjogren, S., and Leck, C. 2013. Cloud and boundary layer interactions over the Arctic sea ice in late summer. *Atmospheric Chemistry and Physics*, **13**(18), 9379–9399.

Siebesma, A. P., and Cuijpers, J. W. M. 1995. Evaluation of parametric assumptions for shallow cumulus convection. *J. Atmos. Sci.*, **52**, 650–666.

Siebesma, A. P., Bretherton, C. S., Brown, A., Chlond, A., Cuxart, J., Duynkerke, P. G., Jiang, H. L., Khairoutdinov, M., Lewellen, D., Moeng, C. H., Sanchez, E., Stevens, B., and Stevens, D. E. 2003. A large eddy simulation intercomparison study of shallow cumulus convection. *Journal of the Atmospheric Sciences*, **60**(10), 1201–1219.

Siebesma, A. Pier, Soares, Pedro M. M., and Teixeira, Joao. 2007. A Combined Eddy-Diffusivity Mass-Flux Approach for the Convective Boundary Layer. *Journal of the Atmospheric Sciences*, **64**(4), 1230–1248.

Simmons, A J, and Hollingsworth, A. 2002. Some aspects of the improvement in skill of numerical weather prediction. *Quarterly Journal of the Royal Meteorological Society*, **128**(580), 647–677.

Smythe, W. R. 1962. Charged right circular cylinder. *J. Appl. Phys*, **33**.

Sobel, Adam H, and Bretherton, Christopher S. 2000. Modeling tropical precipitation in a single column. *Journal of Climate*, **13**(24), 4378–4392.

Soden, B J, and Held, I.M. 2006. An assessment of climate feedbacks in coupled ocean-atmosphere models. *J. Climate*, **19**(14), 3354–3360.

Soden, Brian J., Held, Isaac M., Colman, Robert, Shell, Karen M., Kiehl, Jeffrey T., and Shields, Christine A. 2008. Quantifying Climate Feedbacks Using Radiative Kernels. *J. Climate*, **21**(14), 3504–3520.

Sommeria, G., and Deardorff, J. W. 1977. Subgrid-Scale Condensation in Models of Nonprecipitating Clouds. *Journal of the Atmospheric Sciences*, **34**(2), 344–355.

Stensrud, D.J. 2007. *Parameterization Schemes: Keys to Understanding Numerical Weather Prediction Models.* Cambridge University Press.

Stephens, G. L., Li, J., Wild, M., Clayson, C.A., Loeb, N., Kato, S., L'Ecuyer, T., Stackhouse Jr, P.W., Lebsock, M., and Andrews, T. 2012a. An update on Earth's energy balance in light of the latest global observations. *Nature Geoscience*, **5**, 691–696.

Stephens, Graeme L. 1994. *Remote Sensing of the Lower Atmosphere: An Introduction.* Oxford University Press.

Stephens, Graeme L. 2005. Cloud Feedbacks in the Climate System: A Critical Review. *Journal of Climate*, **18**(2), 237–273.

Stephens, Graeme L., L'Ecuyer, Tristan, Forbes, Richard, Gettlemen, Andrew, Golaz, Jean-Christophe, Bodas-Salcedo, Alejandro, Suzuki, Kentaroh, Gabriel, Philip, and Haynes, John. 2010. Dreary state of precipitation in global models. *Journal of Geophysical Research*, **115**(D24), D24211.

Stephens, Graeme L, Li, Juilin, Wild, Martin, Clayson, Carol Anne, Loeb, Norman, Kato, Seiji, L'Ecuyer, Tristan, Stackhouse, Paul W, Lebsock, Matthew, and Andrews, Timothy. 2012b. An update on Earth's energy balance in light of the latest global observations. *Nature Geosci*, **5**(10), 691–696.

Stephens, Graeme L, Brien, Denis O, Webster, Peter J, Pilewski, Peter, Kato, Seiji, and Li, Jui-lin. 2015. The albedo of Earth. *Reviews of Geophysics*, 141–163.

Stevens, B. 2005. Atmospheric Moist Convection. *Annual Review of Earth and Planetary Sciences*, **33**(1), 605–643.

Stevens, B. 2006. Bulk boundary-layer concepts for simplified models of tropical dynamics. *Theor. Comput. Fluid. Dyn.*

Stevens, B. 2007. On the growth of layers of nonprecipitating cumulus convection. *J. Atmos. Sci.*, **64**, 2916–2931.

Stevens, B. 2015. Rethinking the lower bound on aerosol radiative forcing. *J. Climate*, **28**, 4794–4819.

Stevens, B., and Bony, S. 2016. Water in the Atmosphere. *Physics Today*, **66**.

Stevens, B., Moeng, C.-H., Ackerman, A. S., Bretherton, C. S., Chlond, A., de Roode, S. R., Edwards, J., Golaz, J.-C., Jiang, H., Khairoutdinov, M., Kirkpatrick, M. P., Lewellen, D. C., Lock, A., Müller, F., Stevens, D. E., Whelan, E., and Zhu., P. 2005. Evaluation of large-eddy simulations via observations of nocturnal marine stratocumulus. *Mon. Weather Rev.*, **133**, 1443–1462.

Stevens, Bjorn. 2000. Quasi-Steady Analysis of a PBL Model with an Eddy-Diffusivity Profile and Nonlocal Fluxes. *MWR*, **128**(03), 824–836.

Stevens, Bjorn, and Bony, Sandrine. 2013. Water in the atmosphere. *Physics Today*, 29–34.

Stevens, Bjorn, and Schwartz, Stephen E. 2012. Observing and Modeling Earth's Energy Flows. *Surveys in Geophysics*, **33**(3-4), 779–816.

Stevens, Bjorn, Sherwood, Steven C., Bony, Sandrine, and Webb, Mark J. 2016. Prospects for narrowing bounds on Earth's equilibrium climate sensitivity. *Earth's Future*, **4**(11), 512–522. 2016EF000376.

Stier, P. 2016. Limitations of passive remote sensing to constrain global cloud condensation nuclei. *Atmos. Chem. Phys.*, **16**, 6595–6607.

Stier, P., Feichter, J., Kinne, S., Kloster, S., Vignati, E., Wilson, J., Balkanski, Y., Schulz, M., Ganzeveld, L., Werner, M., I.Tegen, Boucher, O., Minikin, A., and Petzold, A. 2005. The aerosol-climate model ECHAM5-HAM. *Atmos. Chem. Phys.*, **5**, 1125–1156.

Stohl, A., Aamaas, B., Amann, M., Baker, L. H., Bellouin, N., Berntsen, T. K., Boucher, O., Cherian, R., Collins, W., Daskalakis, N., Dusinska, M., Eckhardt, S., Fuglestvedt, J. S., Harju, M., Heyes, C., Hodnebrog, Ø., Hao, J., Im, U., Kanakidou, M., Klimont, Z., Kupiainen, K., Law, K. S., Lund, M. T., Maas, R., MacIntosh, C. R., Myhre, G., Myriokefalitakis, S., Olivie, D. J., Quaas, J., Quennehen, B., Raut, J.-C., Rumbold, S., Samset, B. H., Schulz, M., Seland, Ø., Shine, K. P., Skeie, R. B., Wang, S., Yttri, K. E., , and Zhu, T. 2015. Evaluating the Climate and Air Quality Impacts of Short-Lived Pollutants. *Atmos. Chem. Phys.*, **15**, 10529–10566.

Straka, J.M. 2009. *Cloud and Precipitation Microphysics: Principles and Parameterizations*. Cambridge University Press.

Stubenrauch, C. J., Rossow, W. B., Kinne, S., Ackerman, S., Cesana, G., Chepfer, H., Girolamo, L. Di, Getzewich, B., Guignard, A., Heidinger, A., Maddux, B. C., Menzel, W. P., Minnis, P., Pearl, C., Platnick, S., Poulsen, C., Riedi, J., Sun-Mack, S., Walther, A., Winker, D., Zeng, S., and Zhao, G. 2013. Assessment of Global Cloud Datasets from Satellites: Project and Database Initiated by the GEWEX Radiation Panel. *Bulletin of the American Meteorological Society*, **94**(7), 1031–1049.

Stull, R. B. 1988. *An Introduction to Boundary Layer Meteorology*. The Netherlands: Kluwer Academic Publishers. 666 pp.

Sušelj, Kay, Teixeira, João, and Chung, Daniel. 2013. A unified model for moist convective boundary layers based on a stochastic eddy-diffusivity/mass-flux parameterization. *J. Atmos. Sci.*, **70**(7), 1929–1953.

Suzuki, K., Stephens, G., van den Heever, S., and Nakajima, T. 2011. Diagnosis of the Warm Rain Process in Cloud-Resolving Models Using Joint CloudSat and MODIS Observations. *J. Atmos. Sci.*, **68**, 2655–2670.

Tao, W-K., and Adler, R. 2013. *Cloud Systems, Hurricanes, and the Tropical Rainfall Measuring Mission (TRMM) - A tribute to Dr. Joanne Simpson. Meteorological Monographs.* Vol. 29. American Meteorological Society.

Tao, W.-K., Chen, J.-P., Li, Z., Wang, C., and Zhang, C. 2012. Impact of aerosols on convective clouds and precipitation. *Rev. Geophys.*, **50**, RG2001.

Tawfik, A. B., and Dirmeyer, P. A. 2014. A process-based framework for quantifying the atmospheric preconditioning of surface-triggered convection. *Geophysical Research Letters*, **41**, 173–178.

Taylor, K. E. 2001. Summarizing multiple aspects of model performance in a single diagram. *Journal of Geophysical Research*, **106**, 7183–7192.

Teixeira, J., Cardoso, S., Bonazzola, M., Cole, J., DelGenio, A., DeMott, C., Franklin, C., Hannay, C., Jakob, C., Jiao, Y., Karlsson, J., Kitagawa, H., K hler, M., Kuwano-Yoshida, A., LeDrian, C., Li, J., Lock, A., Miller, M. J., Marquet, P., Martins, J., Mechoso, C. R., Meijgaard, E. v, Meinke, I., Miranda, P. M. A., Mironov, D., Neggers, R., Pan, H. L., Randall, D. A., Rasch, P. J., Rockel, B., Rossow, W. B., Ritter, B., Siebesma, A. P., Soares, P M M, Turk, F. J., Vaillancourt, P. A., Von Engeln, A., and Zhao, M. 2011. Tropical and Subtropical Cloud Transitions in Weather and Climate Prediction Models: The GCSS/WGNE Pacific Cross-Section Intercomparison (GPCI). *Journal of Climate*, **24**(20), 5223–5256.

Tennekes, H. 1973. A model for the dynamics of the inversion above a convective layer. *J. Atmos. Sci.*, **30**, 558–567.

Thorsen, Tyler J., Fu, Qiang, and Comstock, Jennifer M. 2013. Cloud effects on radiative heating rate profiles over Darwin using ARM and A-train radar/lidar observations. *Journal of Geophysical Research: Atmospheres*, **118**(11), 5637–5654.

Tiedtke, M. 1989. A Comprehensive Mass Flux Scheme for Cumulus Parameterization in Large-Scale Models. *Monthly Weather Review*, **117**(8), 1779–1800.

Tiedtke, M. 1993. Representation of Clouds in Large-Scale Models. *Monthly Weather Review*, **121**(11), 3040–3061.

Tjernström, M., Leck, C., Birch, C. E., Bottenheim, J. W., Brooks, B. J., Brooks, I. M., Bäcklin, L., Chang, R. Y.-W., de Leeuw, G., Di Liberto, L., de la Rosa, S., Granath, E., Graus, M., Hansel, A., Heintzenberg, J., Held, A., Hind, A., John-

ston, P., Knulst, J., Martin, M., Matrai, P. A., Mauritsen, T., Müller, M., Norris, S. J., Orellana, M. V., Orsini, D. A., Paatero, J., Persson, P. O. G., Gao, Q., Rauschenberg, C., Ristovski, Z., Sedlar, J., Shupe, M. D., Sierau, B., Sirevaag, A., Sjogren, S., Stetzer, O., Swietlicki, E., Szczodrak, M., Vaattovaara, P., Wahlberg, N., Westberg, M., and Wheeler, C. R. 2014. The Arctic Summer Cloud Ocean Study (ASCOS): overview and experimental design. *Atmospheric Chemistry and Physics*, **14**(6), 2823–2869.

Tomita, H., Miura, H., Iga, S., Nasuno, T., and Satoh, M. 2005. A global cloud-resolving simulation: Preliminary results from an aqua planet experiment. *Geophysical Research Letters*, **32**(8), L08805.

Tompkins, A. M. 2002. A prognostic parameterization for the subgrid-scale variability of water vapor and clouds in large-scale models and its use to diagnose cloud cover. *J. Atmos. Sci.*, **59**, 1917–1942.

Trenberth, K. E., and Fasullo, J. T. 2010. Simulation of present-day and twenty-first century energy budgets of the Southern Ocean. *J. Climate*, **23**, 440–454.

Trenberth, Kevin E, Fasullo, John T, and Kiehl, Jeffrey. 2009. Earth's Global Energy Budget. *Bulletin of the American Meteorological Society*, **90**(3), 311–323.

Troen, I. B., and Mahrt, L. 1986. A simple model of the atmospheric boundary layer; sensitivity to surface evaporation. *Boundary-Layer Meteorology*, **37**(1), 129–148.

Tselioudis, G., and Jakob, C. 2002. Evaluation of midlatitude cloud properties in a weather and a climate model: Dependence on dynamic regime and spatial resolution. *J. Geophys. Res.*, **107**(D24), 4781, doi:10.1029/2002JD002259.–doi:10.1029–2002JD002259.

Tselioudis, G., and Rossow, W. B. 2006. Climate feedback implied by observed radiation and precipitation changes with midlatitude storm strength and frequency. *Geophys. Res. Lett.*, **33**, L02704, doi:10.1029/2005GL024513.

Tselioudis, G., Zhang, Y., and Rossow, W. B. 2000. Cloud and radiation variations associated with northern midlatitude low and high sea level pressure regimes. *J. Climate*, **13**, 312–327.

Tselioudis, G., Lipat, B. R., Konsta, D., Grise, K. M., and Polvani, L. M. 2016. Midlatitude cloud shifts, their primary link to the Hadley cell, and their diverse radiative effects. *Geophys. Res. Lett.*, **43**, 4594–4601.

Tselioudis, George, Rossow, William, Zhang, Yuanchong, and Konsta, Dimitra. 2013. Global Weather States and Their Properties from Passive and Active Satellite Cloud Retrievals. *Journal of Climate*, **26**(19), 7734–7746.

Twomey, S. 1974. Pollution and the planetary albdeo. *Atmos. Environ.*, **8**, 1251–1258.

Twomey, S. 1977. The influence of pollution on the shortwave albedo of clouds. *J. Atmos. Sci.*, **34**, 1149–1152.

Uttal, Taneil, Curry, Judith A., Mcphee, Miles G., Perovich, Donald K., Moritz, Richard E., Maslanik, James A., Guest, Peter S., Stern, Harry L., Moore, James A., Turenne, Rene, Heiberg, Andreas, Serreze, Mark C., Wylie, Donald P., Persson, Ola G., Paulson, Clayton A., Halle, Christopher, Morison, James H., Wheeler, Patricia A., Makshtas, Alexander, Welch, Harold, Shupe, Matthew D., Intrieri, Janet M., Stamnes, Knut, Lindsey, Ronald W., Pinkel, Robert, Pegau, W. Scott, Stanton, Timothy P., and Grenfeld, Thomas C. 2002. Surface Heat Budget of the Arctic Ocean. *Bulletin of the American Meteorological Society*, **83**(2), 255–275.

Vallis, G. K., Zurita-Gotor, P., Cairns, C., and Kidston, J. 2015. Response of the large-scale structure of the atmosphere to global warming. *Q. J. Royal Meteorol. Soc.*, **141**, 1479–1501.

Vallis, Geoffrey K. 2006. *Atmospheric and Ocean Fluid Dynamics: Fundamentals and Large-Scale Circulation*. Cambridge University Press.

van de Hulst, H. C. 1980. *Light scattering by small particles*. Dover.

van der Ent, R. J., Savenije, H. H. G., Schaefli, B., and Steele-Dunne, S. C. 2010. Origin and fate of atmospheric moisture over continents. *Water Resources Research*, **46**.

Van Heerwaarden, C. C., and Vilà Guerau de Arellano, J. 2008. Relative humidity as an indicator for cloud formation over heterogeneous land surfaces. *J. Atmos. Sci.*, **65**, 3263–3277.

VanZanten, M. C., Duynkerke, P. G., and Cuijpers, J. W. M. 1999. Entrainment parameterization in convective boundary layers. *J. Atmos. Sci.*, **56**, 813–828.

Vial, Jessica, Dufresne, Jean-Louis, and Bony, Sandrine. 2013. On the interpretation of inter-model spread in CMIP5 climate sensitivity estimates. *Climate Dyn.*, **41**(11-12), 3339–3362.

Vihma, T., Pirazzini, R., Fer, I., Renfrew, I. A., Sedlar, J., Tjernström, M., Lüpkes, C., Nygård, T., Notz, D., Weiss, J., Marsan, D., Cheng, B., Birnbaum, G., Gerland, S., Chechin, D., and Gascard, J. C. 2014. Advances in understanding and parameterization of small-scale physical processes in the marine Arctic climate system: a review. *Atmospheric Chemistry and Physics*, **14**(17), 9403–9450.

Vilà-Guerau de Arellano, J., van Heerwaarden, C. C., van Stratum, B. J. J., and van den Dries, K. 2015. *Atmospheric boundary layer: Integrating air chemistry and land interactions*. Cambridge University Press.

Vila-Guerau de Arellano, J., van Heerwaarden, C. C., van Stratum, B. J. H., and van den Dries, K. 2015. *Atmospheric boundary layer: Integrating air chemistry and land interactions*. Cambridge University Press.

Voigt, Aiko, Stevens, Bjorn, Bader, Jürgen, and Mauritsen, Thorsten. 2013. The Observed Hemispheric Symmetry in Reflected Shortwave Irradiance. *Journal of Climate*, **26**(2), 468–477.

Wakimoto, R. M., and Srivastava, R. 2003. *Radar and Atmospheric Science: A Collection of Essays in Honor of David Atlas, Meteorological Monographs*. Vol. 30. American Meteorological Society.

Walker, Christopher C., and Schneider, Tapio. 2006. Eddy Influences on Hadley Circulations: Simulations with an Idealized GCM. *Journal of the Atmospheric Sciences*, **63**(12), 3333–3350.

Webb, M., Senior, C., Bony, S., and Morcrette, J.-J. 2001. Combining ERBE and ISCCP data to assess clouds in the Hadley Centre, ECMWF and LMD atmospheric climate models. *Climate Dynamics*, **17**, 905–922.

Weitkamp, Claus. 2005. *Lidar: Range-resolved optical remote sensing of the atmosphere*. Springer.

Wendisch, M., and Brenguier, J.-l. (Eds.). 2013. *Airborne Measurements for Environmental Research: Methods and Instruments., vol.* ISBN: Wiley-VCH Verlag GmbH & Co, Weinheim, Germany.

Westbrook, C. D., Hogan, R. J, and Illingworth, A. J. 2008. The Capacitance of Pristine Ice Crystals and Aggregate Snowflakes. *J. Atmos. Sci*, **65**, 206–219.

Wexler, H. 1936. Coolin in the lower atmosphere and the structure of polar continental air. *Monthly Weather Review*, **64**(4), 122–136.

Wheeler, Matthew C, and Hendon, Harry H. 2004. An all-season real-time multivariate MJO index: Development of an index for monitoring and prediction. *Monthly Weather Review*, **132**(8), 1917–1932.

Wild, M., Gilgen, H., Roesch, A., Ohmura, A., Long, C. N., Dutton, E. G., Forgan, B., Kallis, A., Russak, V., and Tsvetkov, A. 2005. From dimming to brightening: Decadal changes in solar radiation at Earth's surface. *Science*, **308**, 847–850.

Wild, Martin, Folini, Doris, Hakuba, Maria Z, Schär, Christoph, Seneviratne, Sonia I, Kato, Seiji, Rutan, David, Ammann, Christof, Wood, Eric F, and König-Langlo, Gert. 2015. The energy balance over land and oceans: an assessment based on direct observations and CMIP5 climate models. *Climate Dynamics*, **44**(11), 3393–3429.

Wilks, D. S. 2011. *Statistical Methods in the Atmospheric Sciences*.

Williams, K. D., Bodas-Salcedo, A., Déqué, M, Fermepin, S., Medeiros, B, Watanabe, M, Jakob, C., Klein, S. A., Senior, C. A., and Williamson, D. L. 2013. The Transpose-AMIP II Experiment and Its Application to the Understanding of Southern Ocean Cloud Biases in Climate Models. *Journal of Climate*, **26**(10), 3258–3274.

Wilson, D.K. 2001. An alternative function for the wind and temperature gradients in unstable surface layers. *Boundary Layer Meteorology*, **99**, 151–158.

Wing, A. A., Emanuel, K., Holloway, C. E., and Muller, C. 2017. Convective self-aggregation in numerical simulations: A review. *Surveys in Geophysics*, **38**, 1173–1197.

WMO. 2017. *International Cloud Atlas: Manual on the Observation of Clouds and Other Meteors*. `https://cloudatlas.wmo.int/home.html`. [Online; accessed 13-Nov-2017].

Wood, R. 2007. Cancellation of aerosol indirect effects in marine stratocumulus through cloud thinning. *J. Atmos. Sci.*, **64**, 2657–2669.

Wood, R. 2012. Stratocumulus clouds. *Mon. Weather Rev.*, **140**, 2373–2423.

Wood, R., and Bretherton, C. S. 2004. Boundary layer depth, entrainment, and decoupling in the cloud-capped subtropical and tropical marine boundary layer. *J. Climate*, **17**, 3576–3588.

Wood, Robert, and Field, Paul R. 2011. The Distribution of Cloud Horizontal Sizes. *Journal of Climate*, **24**(18), 4800–4816.

Wyant, Matthew C, Bretherton, Christopher S, Chlond, Andreas, Griffin, Brian M, Kitagawa, Hiroto, Lappen, Cara-Lyn, Larson, Vincent E, Lock, Adrian, Park, Sungsu, de Roode, Stephan R, Uchida, Junya, Zhao, Ming, and Ackerman, Andrew S. 2007. A single-column model intercomparison of a heavily drizzling stratocumulus-topped boundary layer. *J. Geophys. Res.*, **112**(D24), D24204–n/a.

Wyngaard, John C. 2010. *Turbulence in the Atmosphere*. Cambridge, UK: Cambridge University Pess.

Yanai, Michia, Esbensen, Steven, and Chu, Jan-Hwa. 1973. Determination of bulk properties of tropical cloud clusters from large-scale heat and moisture budgets. *Journal of the Atmospheric Sciences*, **30**, 611–627.

Zelinka, Mark D., and Hartmann, Dennis L. 2010. Why is longwave cloud feedback positive? *J. Geophys. Res.*, **115**(D16). D16117.

Zelinka, Mark D., Klein, Stephen A., and Hartmann, Dennis L. 2012. Computing and Partitioning Cloud Feedbacks Using Cloud Property Histograms. Part II: Attribution to Changes in Cloud Amount, Altitude, and Optical Depth. *J. Climate*, **25**(11), 3736–3754.

Zelinka, Mark D, Klein, Stephen A, Taylor, Karl E, Andrews, Timothy, Webb, Mark J, Gregory, Jonathan M, and Forster, Piers M. 2013. Contributions of Different Cloud Types to Feedbacks and Rapid Adjustments in CMIP5. *J. Climate*, **26**(14), 5007–5027.

Zhang, Chidong. 2005. Madden-julian oscillation. *Reviews of Geophysics*, **43**(2).

Zhang, Guang J. 2002. Convective quasi-equilibrium in midlatitude continental environment and its effect on convective parameterization. *Journal of Geophysical Research: Atmospheres*, **107**(D14), ACL 12–1–ACL 12–16.

Zhang, Guang J. 2003. Convective quasi-equilibrium in the tropical western Pacific: Comparison with midlatitude continental environment. *Journal of Geophysical Research: Atmospheres*, **108**(D19).

Zhang, M., Bretherton, C. S., Blossey, P. N., Austin, P. H., Bacmeister, J. T., Bony, S., Brient, F., Cheedela, S. K., Cheng, A., Genio, A. D. Del, De Roode, S. R., Endo, S., Franklin, C. N., Golaz, J.-C., Hannay, C., Heus, T., Isotta, F. A., Dufresne, J.-L., Kang, I.-S., Kawai, H., Köhler, M., Larson, V. E., Liu, Y., Lock, A. P., Lohmann, U., Khairoutdinov, M. F., Molod, A. M., Neggers, R. A. J., Rasch, P., Sandu, I., Senkbeil, R., Siebesma, A. P., Siegenthaler-Le Drian, C., Stevens, B., Suarez, M. J., Xu, K.-M., von Salzen, K., Webb, M. J., Wolf, A., and Zhao, M. 2013. CGILS: Results from the first phase of an international project to understand the physical mechanisms of low cloud feedbacks in single column models. *J. Adv. Model. Earth Syst.*, 826–842.

Zipser, Edward. 1969. The role of organized unsaturated downdrafts in the structure and rapid decay of an equatorial disturbance. *Journal of Applied Meteorology*, **8**, 799–814.

Zygmuntowska, M., Mauritsen, T., Quaas, J., and Kaleschke, L. 2012. Arctic Clouds and Surface Radiation ĂćâĆňâĂIJ a critical comparison of satellite retrievals and the ERA-Interim reanalysis. *Atmospheric Chemistry and Physics*, **12**(14), 6667–6677.